ANALYSIS OF PERFORMANCE CHARACTERISTICS OF ELECTRIC VEHICLE TRACTION DRIVE IN LOW SPEED/LOW TORQUE RANGE

Heath E. Kouns

Thesis submitted to the faculty of the Virginia Polytechnic Institute and State University
In partial fulfillment of the requirements for the degree of

Master of Science
in
Electrical Engineering

Presented to:

Dr. Jason Lai (Chair)

Dr. Charles Konrad

Dr. Dan Chen

December 6, 2001
Blacksburg, Virginia

Keywords: motor drive, control strategy, maximum efficiency, inverter, torque per ampere and electric vehicle

ANALYSIS OF PERFORMANCE CHARACTERISTICS OF ELECTRIC VEHICLE TRACTION DRIVE IN LOW SPEED/LOW TORQUE RANGE

Heath Kouns

(Abstract)

In a world with a growing population there is a trend toward higher and higher energy usage. Because of the cost involved in producing extra energy, there is a need for more efficient usage of the energy that is already available. The issue of efficiency rings home especially clear with electric motors. Although induction motors are used in many different applications, the motors used in electric vehicles must be able to generate a large starting torque as well as operate over a wide speed range. This work analyzes the restrictions placed on the motor and inverter drive system. It also looks at the best method for controlling the drive in order to achieve the highest efficiency out of the drive. While other works have shown methods of achieve high efficiency out of the motor, it is the assertion of this work that the efficiency of the total drive is more important. It is to that end that this work analyzes the performance of an induction motor under low torque and speed where a traction drive utilizes the most energy.

This work was sponsored by Virginia Power Technologies (VPT) under the DOE CARAT (Cooperative Automotive Research for Advanced Technology) Program.

To my wife

Acknowledgements

To start, I would like to thank my Lord and Savior, Jesus Christ, without whom I would not be where I am today.

I would like to thank my advisor, Dr. Jason Lai, for his patience and continued support while I have been at Va Tech. I will always be grateful to him for his guidance and his instruction in power electronics. I am also grateful to my other committee members, especially, Dr. Charles Konrad for his tremendously valuable help and insight during the course of this work. His knowledge of "real" engineering has shown me that at times it takes more than a formula to make a system work.

I also wish to thank all of the CPES students for their help, especially Xiaoyan Wang, Yuxin Li, George Yu, Francisco Canales, Eric Hertz, Leonard Leslie, Troy Nergaard, Jeremy Ferrell and Robert Gannet. I will not forget the support and guidance they offered during my stay.

I am also thankful to the CPES staff for their assistance and kindness, especially Trish Rose, Elizabeth Tranter, and Bob Martin. I have been honored to be a member of CPES and I will reference the lessons I have learned here for years to come.

To my family, I owe a very large debt of gratitude. My parents have always been there to support me in every decision I have made and to offer guidance, as I needed it. I have gotten to this point in life using the work ethic and logical approach to situations that I was taught growing up. I would like to thank my wife Penny for putting up with my long nights away from home and my non-stop schedule. She has truly sacrificed during our first years of marriage and I promise, I will repay her for her unselfishness. The Lord blessed me a wonderful wife.

Thank you all, for the influence you have had on my life.

Analysis of Performance Characteristics of Electric Vehicle Traction Drive in Low Speed/Low Torque Range

Contents

List of Figures

Chapter 1: Scope of Work

1.1. Introduction

In a world with a growing population there is a trend toward higher and higher energy usage. Because of the cost involved in producing extra energy, there is a need for more efficient usage of the energy that is already available. By improving the ratio of power output to power input for each individual component in the energy "food chain", the existing power plants are enabled to serve a larger segment of customers without increasing capacity. This has beneficial effects for both the economy and the environment.

The issue of efficiency rings home especially clear with electric motors. It is known that 65% of the energy used in the United States of America is consumed by motors. In industry the ratio is even higher at 76%. 90% of the motors that use the energy in industry are induction motors [26]. Induction motors are used because of their ruggedness and reliability. Because there is a vast amount of material that has already been published on the operation and characteristics of an induction machine, they are more apt to be included in new installations if only because of the comfort factor that users have with them. One can also start an induction motor by simple placing it across the line with a contactor, which is a significant advantage.

Another application for induction motors is growing out of a need to preserve fossil fuels. The automotive industry has been looking for a reliable and implementable substitute for petroleum based engines for several years [18]. Whether the power is obtained from a hydrogen fuel cell, a battery, or some other energy storage device, almost all feasible plans will utilize an electric motor to drive the wheels. This motor, called a traction motor, has operational constraints placed on it that are not necessarily

experienced by industrial motors. The attributes of an induction motor make it a good choice for this job. This work analyzes the restrictions placed on the motor and inverter drive system. It also looks at the best method for controlling the drive in order to achieve the highest efficiency out of the drive. While other works have shown methods of achieve high efficiency out of the motor, it is the assertion of this work that the efficiency of the total drive is more important.

1.2. Background

Although induction motors are used in many different applications, the motors used in electric vehicles must be able to generate a large starting torque as well as operate over a wide speed range. An electric vehicle places demands on a motor that many industrial situations do not. For the most part, in the past, motor drives have been optimized to operate with high efficiency at rated torque. While it is important to run efficiently in that region, there are other points at which it is arguably more important to be efficient. It is quite analogous to the case of gasoline engines, where it is known that fuel efficiency goes down with hard acceleration or high speed. That hard acceleration or high speed is an indication of high torque levels being produced by the engine. Most modern gasoline power plants are designed to run optimally at lower torque and speed. Figure 1 shows a standard fuel economy graph. One can see that the engine runs very efficiently at around 20mph, which is not even close to typical highway speeds.

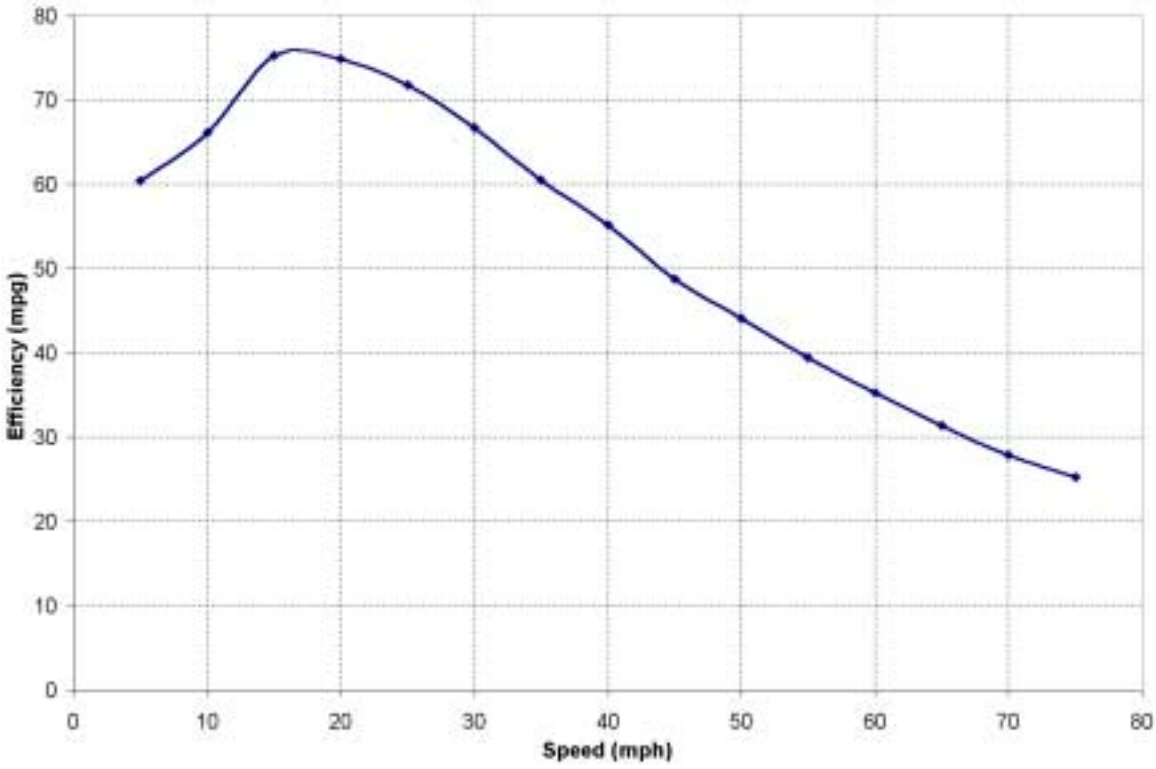

Figure 1 Typical Fuel Economy Profile

In electric vehicle applications the efficiency of the drive is even more important because of the limited fuel supply. The drive should be optimized so that it works the most efficiently at the point at which the drive spends consumes the most energy. From the Federal Urban Driving Schedule (FUDS), the best place to optimize the efficiency of the motor becomes evident. The FUDS was generated some time ago by driving a vehicle around Los Angeles for about 23 minutes while recording the speed and other pertinent information. After this was set as the standard, automobiles could be tested on a dynamometer under the same set of circumstances in order to have a level basis on which to compare vehicles. Figure 2 shows the speed profile of the urban driving schedule. This is interesting in that you can see where the vehicle started and stopped but it only tells part of the story of how the drive was actually loaded. A better view is shown in Figure 3, which shows the torque generated over the 23-minute cycle. The sharp peaks correspond to periods of acceleration. While the drive obviously has to cope with these high points, it also must produce good results along the rest of the cycle as

well and when a trend line is placed on the graph it shows that, for most of the time, the torque occurs between five and ten foot pounds.

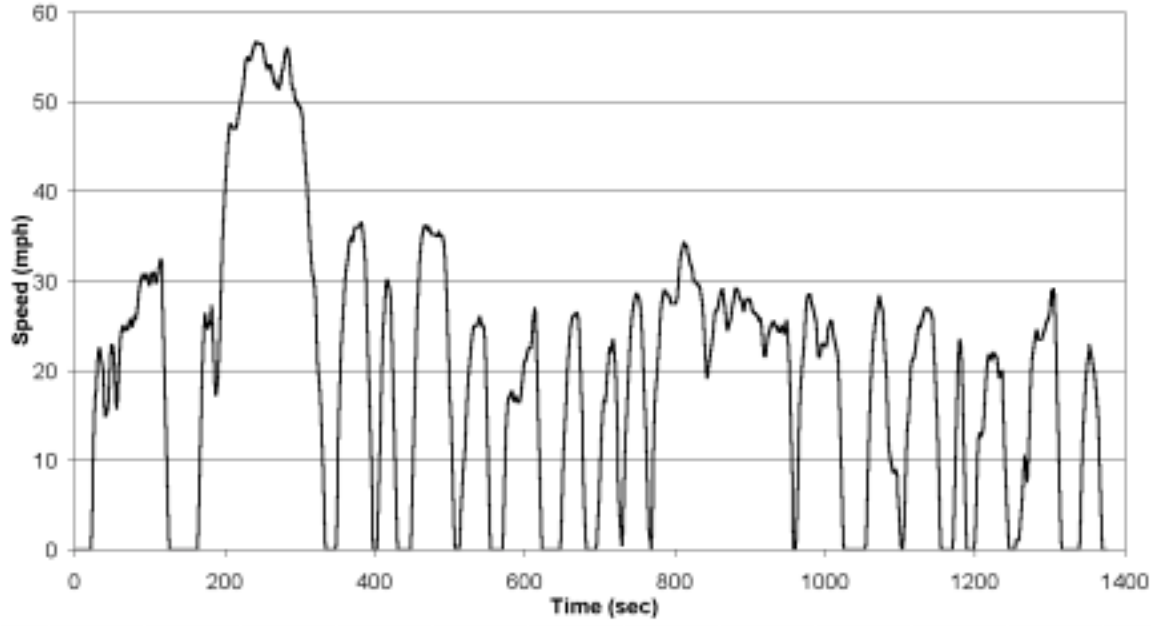

Figure 2 FUDS Speed Profile

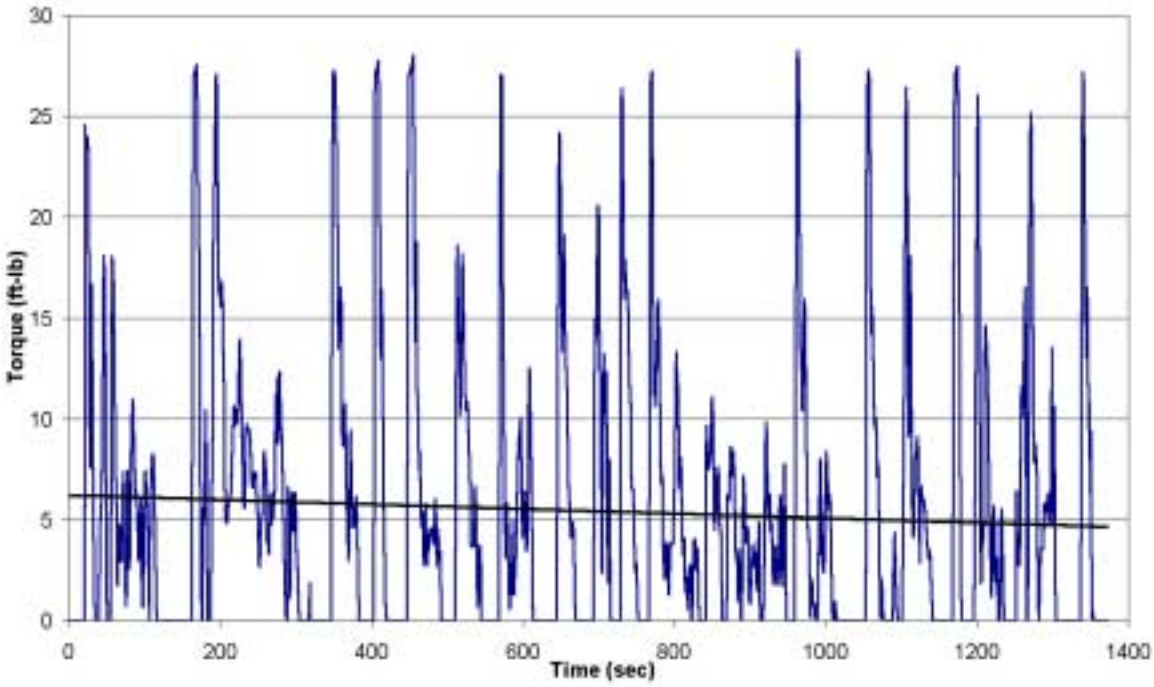

Figure 3 FUDS Torque Profile

More important than the maximum torque produced or the maximum output power available is the amount of energy required because this is what directly determines how long the alternative fuel source will last. If one calculates the power at each instant over the FUD cycle, tabulates the energy used, and then plots the energy usage versus torque, one sees a very distinct trend. Figure 4 shows that in this case about 75% of the energy is used in a band of torque values around 5 and 10 ft-lbs. A local maxima in the plot at 25 ft-lbs corresponds to the torque produced during acceleration.

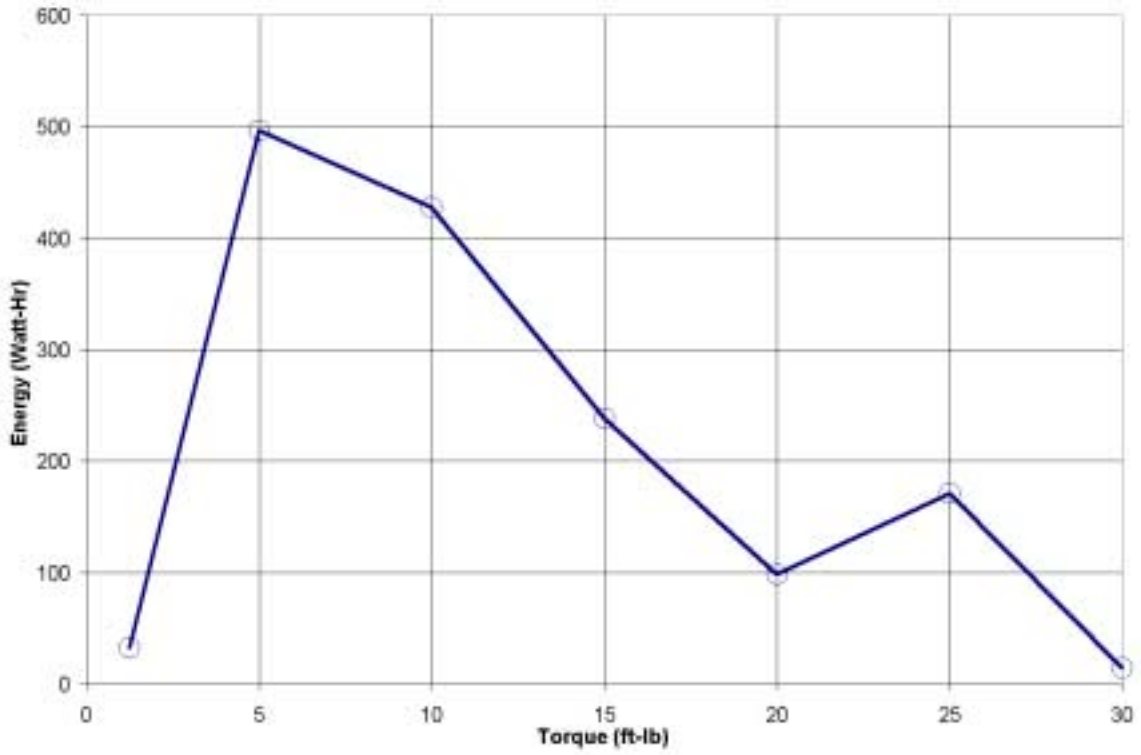

Figure 4 Energy Dissipated vs. Torque for FUDS

The same information is conveyed in Figure 5, which also shows the energy correlation to speed. As an observation, it is also notable that a majority of the energy is not only expended at low torque but at lower speeds as well. Therefore, it follows that the best place to optimize the drive is not at its nameplate ratings but at relatively low values of torque and speed because that is where the drive operates for most of the time. This is contrary to many drives designed and in use today. This partially stems from the point mentioned earlier that many of the induction machine drives in use presently are for industrial applications and many industrial situations call for a drive that is constant

torque or speed and so the machine is sized very close to the operational point and the drive is optimized for that point. In electric vehicle drives, however, the motor must be much larger than is needed for its primary operational point. Although the concept of EV drives has been around for a long time, most of the knowledge base and control methodology currently used has a strong industrial influence [18]. The purpose of this work is to address the need for more analysis in the low speed, low torque region of an induction machine and look at possible control schemes that are the most beneficial in EV applications.

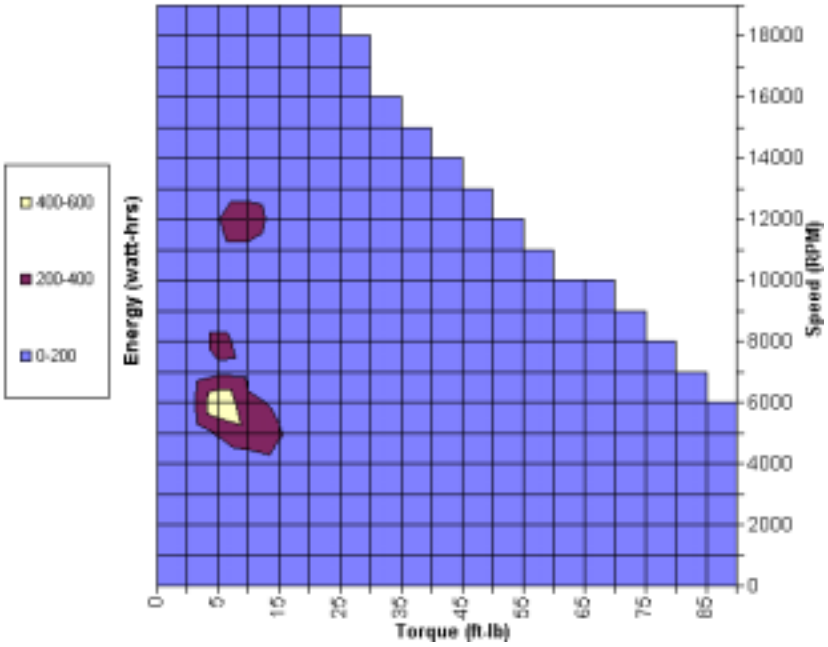

Figure 5 Plot of Energy Usage Versus Torque and Speed

Figure 6 shows the exact data as shown in Figure 5, but displays it in a 3-dimensional format. Notice that the energy usage is very concentrated into two main areas and has localized high points corresponding to specific events such as acceleration in the driving routine.

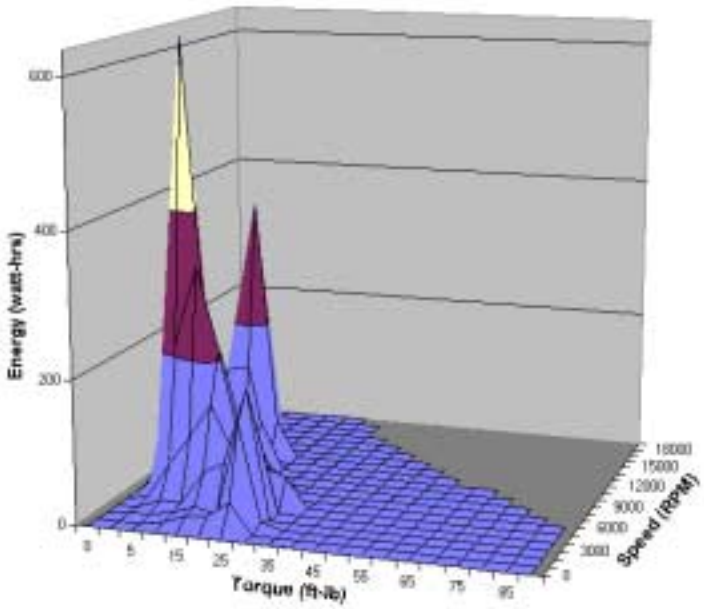

Figure 6 3D Plot of FUDS Energy Usage Versus Torque and Speed

The analysis above covers urban driving very well. However, more and more traveling is being done on interstates, so another standard was developed called US-06. This profile is shown is Figure 7. The average speed is obviously much higher and one can see although the profile only lasts 10 minutes, over six minutes is spent at over 60 mph. However, the interesting point is the average torque is still below 15 ft-lb. Figure 8 show the energy usage over time and although the peaks are at higher speeds as compared to Figure 6, the torque levels at which the peak energy usage occurs is relatively low when compared to the motor's rated torque. This means that the work presented here is warranted under all driving conditions and the resulting conclusions will prove beneficial for a wide variety of operating conditions.

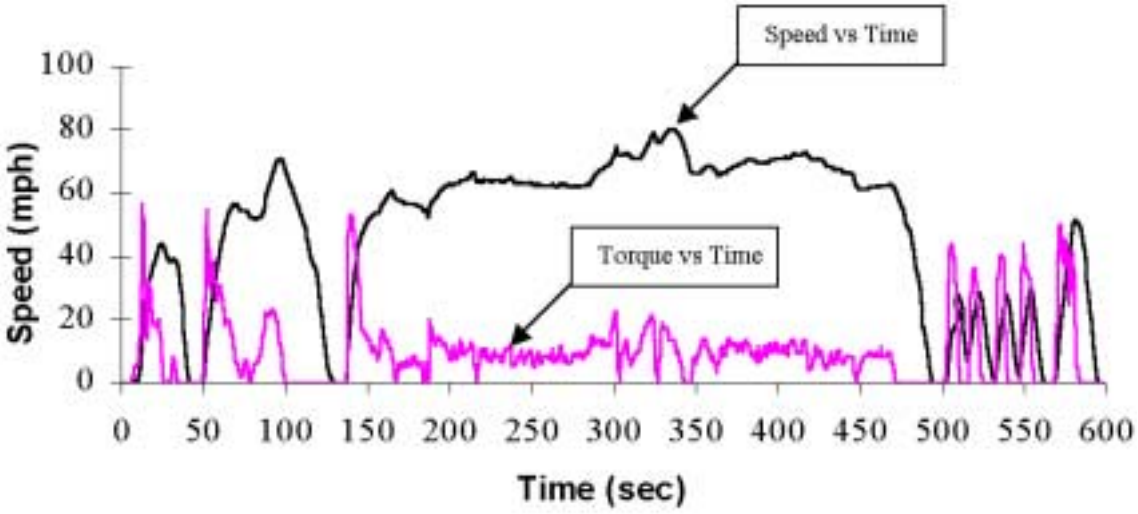

Figure 7 US-06 Speed and Torque Profile

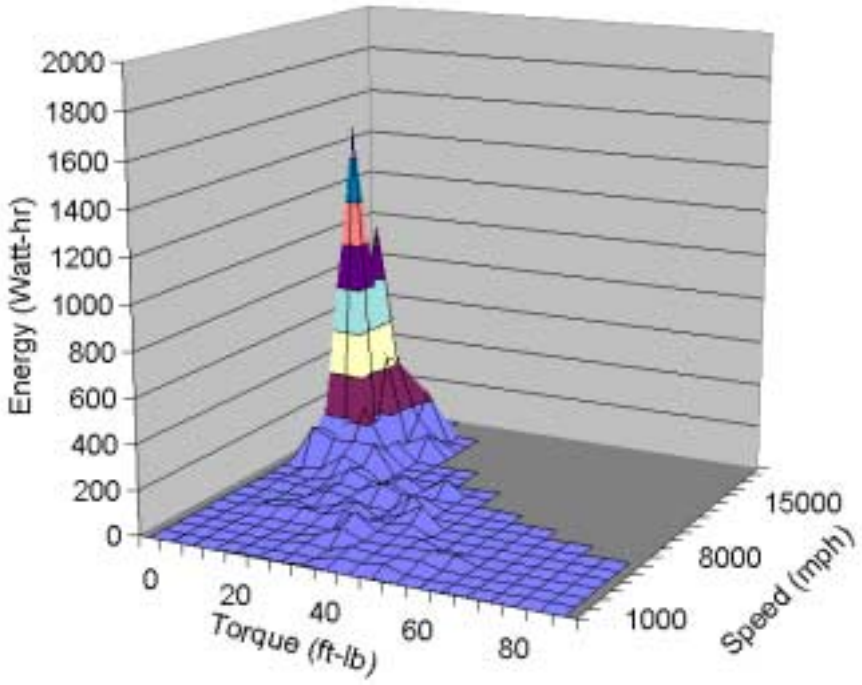

Figure 8 3D Plot of US-06 Energy Usage Versus Torque and Speed

1.3. Motor Control Strategies

There are many complicated control schemes that have been presented and implemented recently that have a common interest. They are all concerned with improving the efficiency of the motor drive system. Although they share a common objective the methods tend to approach the problem from different angles. Most of the methods tend to treat the switching inverter and motor independently, which will not realize the best results. They also tend to apply to motors operating at rated load and speed. This is because much of the material that exists is for motors in an industrial setting rather than an automotive setting. The technology existing for electric vehicles is presented in [18], which reviews the past 25 years of electric vehicle propulsion.

The authors of [24] assert that the converter losses do not need to be included in a maximum efficiency strategy for a medium sized induction motor. The work presented here contradicts that and shows that the best operation point is not at the best efficiency point of the motor.

Many of the methods for efficiency improvement that exist stem from various vector control strategies. The authors of [16] demonstrate a method for obtaining maximum drive efficiency by looking at the third harmonic signal and using it to regulate the flux producing portion of the stator current after it is split up in a vector control strategy. The material in [5] presents a maximum torque per ampere strategy that derives vector relationships that show the optimum slip at which to achieve the optimum efficiency. However in order to simplify the problem, the method ignores core loss effects which can be significant. The work presented here differs by analyzing and showing experimental validation of a model that includes core losses.

Other works, such as [6, 15, 19, 21, 22], have included iron loss models in their analysis but they do not try to optimize the torque per ampere effect. One body of work does attempt to obtain minimum losses in the system by using a “golden section” search technique to look to the optimum value of flux needed to generate a certain torque/speed level. The method, presented in [3], calculates the power using the output currents. However it does not measure the output speed, which introduces a speed error during system transients.

Another control strategy that exists is to optimize the amount of torque produced for a given amount of stator current. This technique is known as maximum torque per ampere. The authors of [14] try to obtain maximum torque per ampere by using a constant volts per hertz ratio. As presented later in this paper, that relationship may not be constant for optimum operation after all. In fact the material in [20] supports this as it demonstrates an optimal efficiency technique that changes the voltage to frequency relationship under low load factor. The technique uses a look-up table developed from measured parameters. A method of improving efficiency by adjusting the voltage to frequency ratio as the operating point of the motor deviates from rated speed and torque is described in [26.] Other torque optimizing strategies exist but they tend not to apply to the situation addressed by a traction drive. The papers [9,11,13] present an optimum torque control strategy but it is for the field-weakening region of an induction motors operation range. This is not the point at which a traction drive spends the most time, which means that there are better places to optimize the efficiency.

1.4. Objectives and Thesis Overview

Because an induction motor in an electric vehicle is operated under conditions that it typically would not face in an industrial application, new control methods must be found that will optimize the motor performance and efficiency for its given task. As demonstrated above, a traction drive spends much of its time at low torque. Typical control schemes have tried to operate the motor with constant volts per hertz or at a point of minimum power loss in the motor. This may not be the best place to operate the traction drive and the thrust of this work is to demonstrate this concept. Results are shown that for a given speed and torque, the point of minimum power loss in the motor does not occur at the same slip frequency at which the best torque per ampere point occurs.

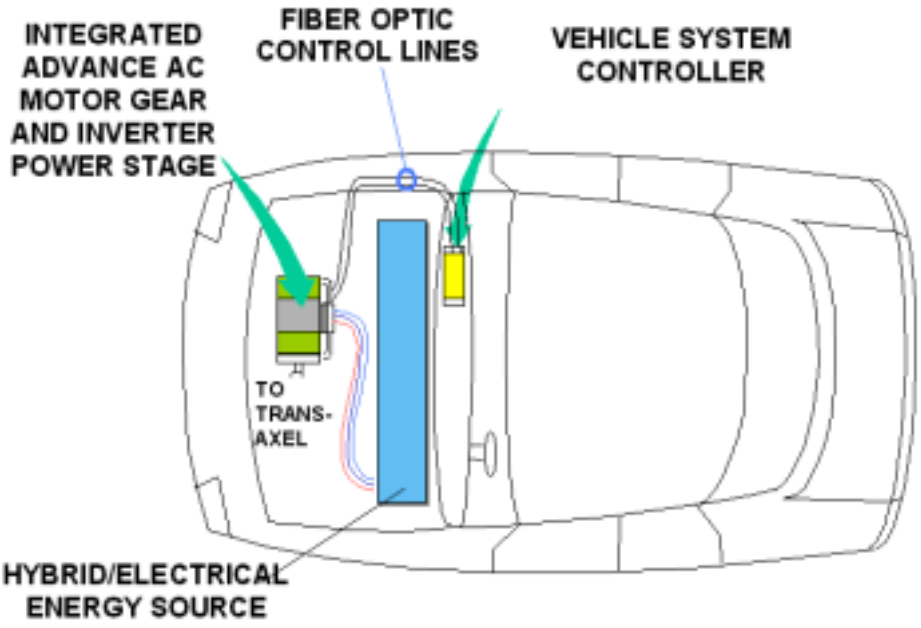

Figure 9 Motor Drive Integration into Electric Vehicle

Chapter Two will demonstrate the points listed above through computer simulation using an analytical software package. The software used throughout this process was Mathcad 8 Professional. The induction motor is analyzed in terms of a scalar circuit. A scalar representation is sufficient to demonstrate the concepts and ideas presented earlier. A program was developed that accurately describes the real world system and it was used to predict the performance and operational characteristics of the test system under various circumstances.

The design and implementation of an experimental test bed is illustrated in Chapter Three. A 75kw inverter was designed and constructed that demonstrated very high levels of integration. This was done to improve efficiency and to produce a more compact package while maintaining a high degree of performance. In fact it is shown that the voltage overshoot is greatly reduced which aids in efficiency as well as device life expectancy. The integration level will allow the traction drive package to save precious space in the motor compartment of next generation electric vehicles. The inverter was used in open loop to drive a specially designed motor that was connected to a dynamometer to allow specific operating conditions to be generated. The test procedure was closely monitored to insure consistency of data.

Next, test results using the drive system are presented and compared to the simulated results. Plots from Mathcad and experimental results are shown. A very close correlation is presented. Because of the accuracy demonstrated by the simulation program, other test criteria may be used and one can feel very comfortable believing the simulation results.

Finally, the thrusts of the thesis are re-examined. The objectives are presented and the results are summarized. Conclusions are drawn regarding how this body of work can be applied to work in the field. Also, ideas for future extensions of this work are presented.

Chapter 2: Analytical Evaluation

2.1. Introduction

Induction motors, especially squirrel cage motors are very rugged and robust, yet they are simple and economical to build. This makes them ideal candidates for traction drive systems in electric vehicle applications [18]. Another advantage of the induction machine design is the volume of work that has already been completed and can be drawn on for information. This information, however, tends to be at rated speed or torque. This is because, a lot of the work that has been completed has been for industrial application where the motor is designed for a specific task and the smallest motor that will generate the needed power is used. The motor used for a traction drive must be able to run efficiently far below its rating as well as run effectively at high torque and speed for start up and acceleration operations. In order to fully prove a hypothesis, analytical as well as experimental validation should be provided. In this case, the motor drive system mentioned in the previous chapter is systematically modeled and simulated using Mathcad. This chapter lays the groundwork for modeling an induction traction motor and then presents results from detailed simulations.

2.2. Model Derivation

Induction machines work on the principle of rotating magnetic fields. In a three-phase motor, three windings are physically placed around the stator with a separation of 120 degrees. Actually, each stator winding is distributed in slots around the periphery in order to reduce the harmonics in the mmf being generated. The harmonics are reduced

the greatest if the distribution is sinusoidal which would lead to a purely sinusoidal mmf. In this work, a sinusoidal distribution is assumed as a simplifying approximation. When three alternating currents (separated by 120 degrees in time) are passed through the coils, the resulting flux density is a traveling wave of mmf and the magnetic field that is produced by this mmf is known as a rotating magnetic field. The magnetic field rotates at what is known as synchronous speed, which is given by:

$$n_s = \frac{120 * f}{P} rpm \qquad \textbf{(2.1)}$$

Where P is the number of poles in the machine.

The rotor winding in a squirrel cage machine is a series of conducting bars laid in slots around the rotor and short-circuited on the ends. When the rotating magnetic field produced by the stator passes through or cuts through the rotor bars, voltages are induced which leads to the creation of rotor currents. The alternating rotor current produces a second rotating magnetic field. The rotating field due to the rotor tries to stay aligned with the field due to the stator and this action causes a torque to be induced on the rotor, which causes the rotor to rotate in the same direction as the rotating magnetic fields. The rotor does not rotate at the same speed as the synchronous speed and the fractional difference is known as slip.

$$s = \frac{n_s - n}{n_s} \qquad \textbf{(2.2)}$$

Because of the magnetic coupling of an induction machine, a common analysis technique is to look at it like a transformer. In fact it is very helpful to use the transformer model when analyzing an induction machine. The main difference is that, unlike a conventional transformer, the frequency of the rotor current is different from the frequency of the stator current. The stator of the motor corresponds to the primary and the rotor is like the secondary. The correlation between the two is through the flux linkage generated by the rotating magnetic fields. This model of an induction machine can be reduced to an equivalent circuit if the rotor quantities are referred to the stator. The standard equivalent circuit for an induction motor is shown Figure 10.

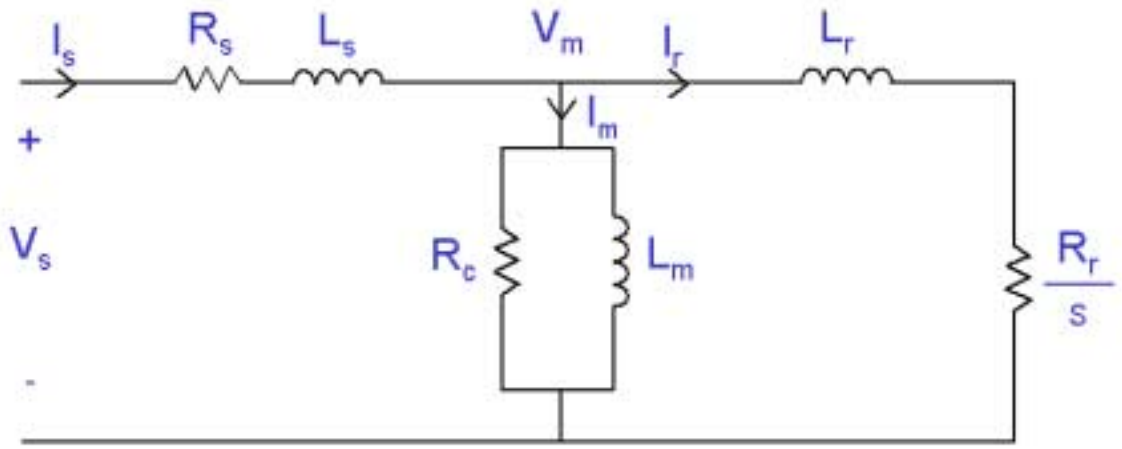

Figure 10 Equivalent Circuit of an Induction Motor

Figure 11 shows the circuit of Figure 10 with the lumped rotor resistance split out into the resistance of the rotor windings and the resistance, which represents the shaft load. It is through this resistance that the power is delivered to the rotor shaft.

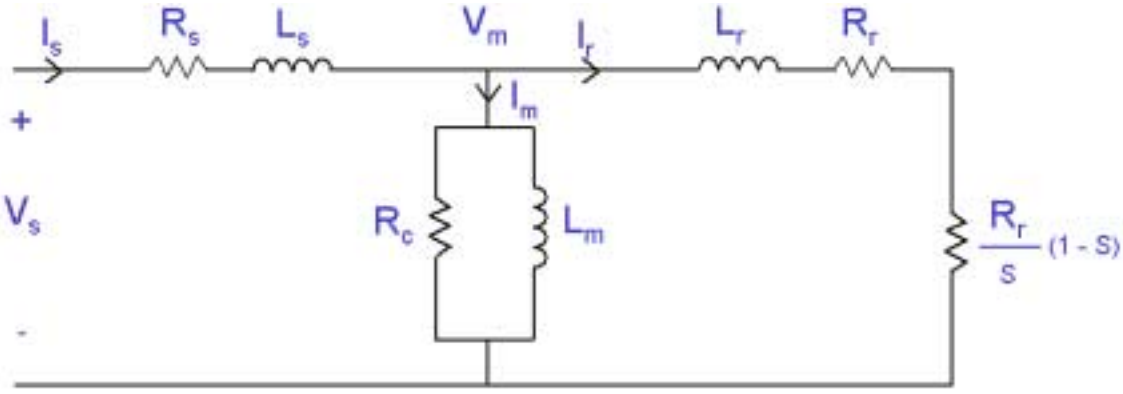

Figure 11 Modified Induction Motor Equivalent Circuit

From this phase leg representation of the motor many important factors can be gleaned. In this work, since the target was to look at the performance at specific speeds and torques, the obvious starting point is the output power. The output power delivered to the shaft is given in (2.3).

$$P_{out} = \frac{746 * T * n}{5252} \qquad \textbf{(2.3)}$$

Where P_{out} is the output power in watts, T is rotor torque in ft-lb and *n* is the rotor speed measured in rpm.

The output power found above is dissipated through the resistor in the equivalent circuit represented by $R_r(1-s)/s$. By using the, I squared R, relationship with power, the rotor current can be found. The three in the denominator is due to the power found above being the total power applied to the rotor, while the equivalent circuit parameters found below and referenced in Figure 10 are per phase quantities.

$$I_r = \sqrt{\frac{s * P_{out}}{3R_r(1-s)}} \quad \textbf{(2.4)}$$

The rotor impedance is the sum of the rotor resistance and the reactance, which varies linearly with line frequency.

$$Z_r = \frac{R_r}{s} + X_r \quad \textbf{(2.5)}$$

By using the results of (2.4) and (2.5), the voltage across the magnetizing branch can be found, as shown below in (2.6).

$$V_m = I_r Z_r \quad \textbf{(2.6)}$$

Because the iron losses vary which include hysterysis and eddy currents vary with frequency, the magnetizing resistance, R_m must be adjusted as it varies as the 1.5 power with line frequency. The magnetizing reactance changes linearly with frequency. Using the magnetizing impedance as well as the voltage across the magnetizing branch found in (2.6), the current flowing through the magnetizing branch can be found.

$$|I_m| = \left|\frac{V_m}{R_m}\right| + \left|\frac{V_m}{X_m}\right| \quad \textbf{(2.7)}$$

Using Kirchoff's current law, the stator current can be found as the sum of the current flowing through the rotor as well as the current being lost through the magnetizing branch.

$$|I_s| = |I_m| + |I_r| \quad \textbf{(2.8)}$$

2.3. Circuit Simulation

The approach taken to simulate the circuit was to use the scalar approximations described above as the basis. Using Mathcad allows one to sequentially step through an analysis and look at the result of each step independently. This provides more freedom than is available in circuit based simulators such as P-Spice or Saber.

One of the leading premises of this work was that by altering the slip at a certain operating point, one is able to improve the efficiency of the motor drive operation. Because of this, in setting up the simulation, the slip frequency was used as the independent variable and it was adjusted over a range that was wide enough to see any significant detail. This proved to be about three hertz.

The first point of significance that was developed using the scalar model for an induction motor was that the point of maximum efficiency for the motor is not the point at which the stator current is minimum. This is demonstrated in Figure 12. (The case shown in the simulation was for the point at which an electric vehicle traction drive spends the majority of its time as established previously.)

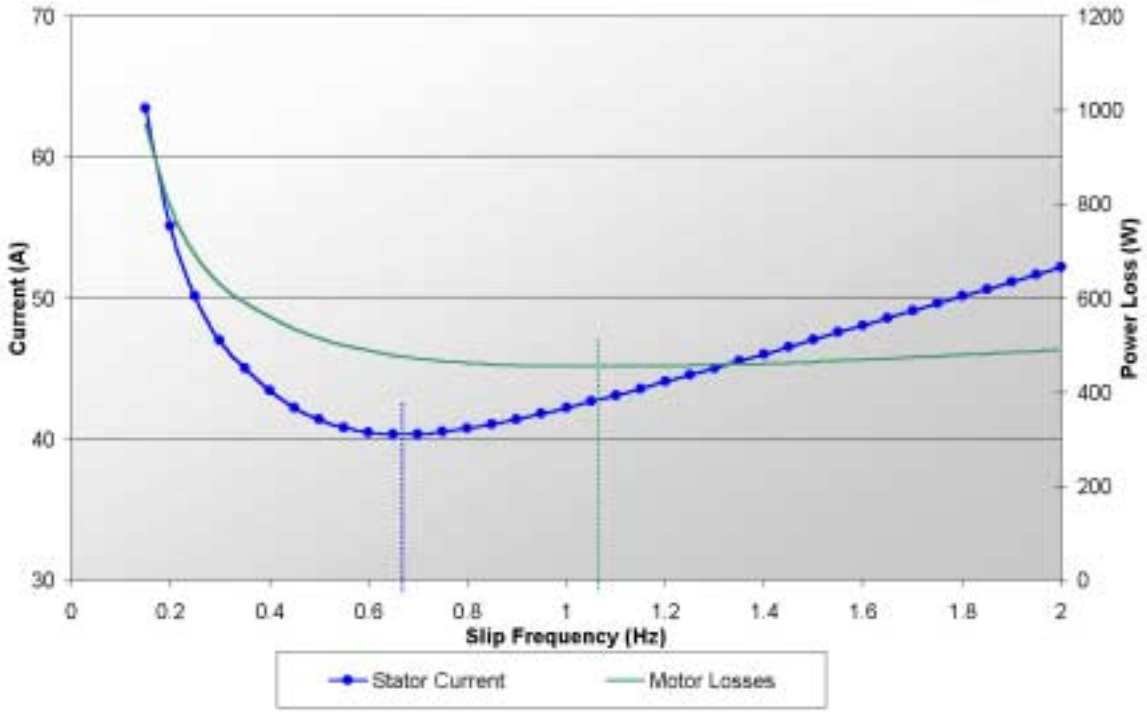

Figure 12 Stator Current and Motor Losses - 3000RPM 5ft-lb

The figure clearly shows that the motor is able to produce the same torque with a minimum stator current at around 0.65Hz. However, even though there is less current being supplied to the motor, it is not being run most efficiently. The highest efficiency or minimum power loss of the motor occurs at a slip frequency of about 1.05Hz. The reason for this difference is the nonlinear relationship between the magnetizing impedance and the voltage applied to each phase of the motor.

In order to make use of these low points in the performance curves, it is necessary to understand how the curves shift under varying operating conditions. If the variations in the minimum points can be accurately predicted then improved control strategies can be more readily implemented. In past work, people have made an effort to make the motor run with the lowest losses and this concept is demonstrated first. The circuit was simulated at a rotor speed of 3000RPM for a range of shaft torques. For each curve shown in Figure 13, the output power remains constant because the torque and rotor speed are held constant and (2.3) dictates that those are the only contributors to the shaft power. Although the output power remains the same the losses in the motor change as the slip frequency is varied. The point that is presented in Figure 13 is that the slip frequency at which the efficiency is highest is independent of torque for a given rotor speed.

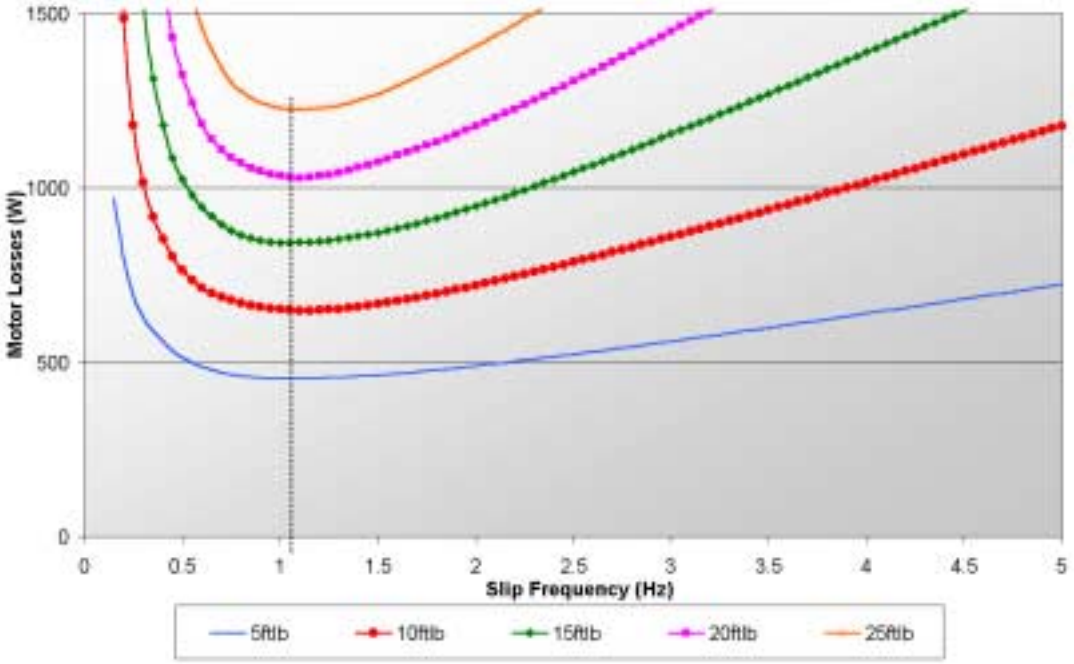

Figure 13 Motor Losses - 3000RPM

This is significant because is means that the characteristics of the losses in the motor are independent of voltage. This is implied because if neither the slip nor the speed changes, yet a higher torque is obtained then the voltage had to be increased. This does not mean that the losses do not increase with voltage, only that the increase is linear. Figure 14 shows the effect of adjusting the rotor speed. The torque was held constant and four different speeds were simulated. The result was that as the speed was increased, for each successive test, the slip at which the minimum losses occurred in the motor also increased. That increase in slip frequency corresponding to maximum efficiency is linear with rotor speed. One interesting point is that if the information in Figure 14 is taken and plotted on a different x-axis, namely percent slip, an interesting trend is observed. Figure 15 shows that the maximum efficiency seems to occur at nearly the same point when the slip frequency is considered as a fraction of the rotor frequency. There does appear to be some variance but it is slight.

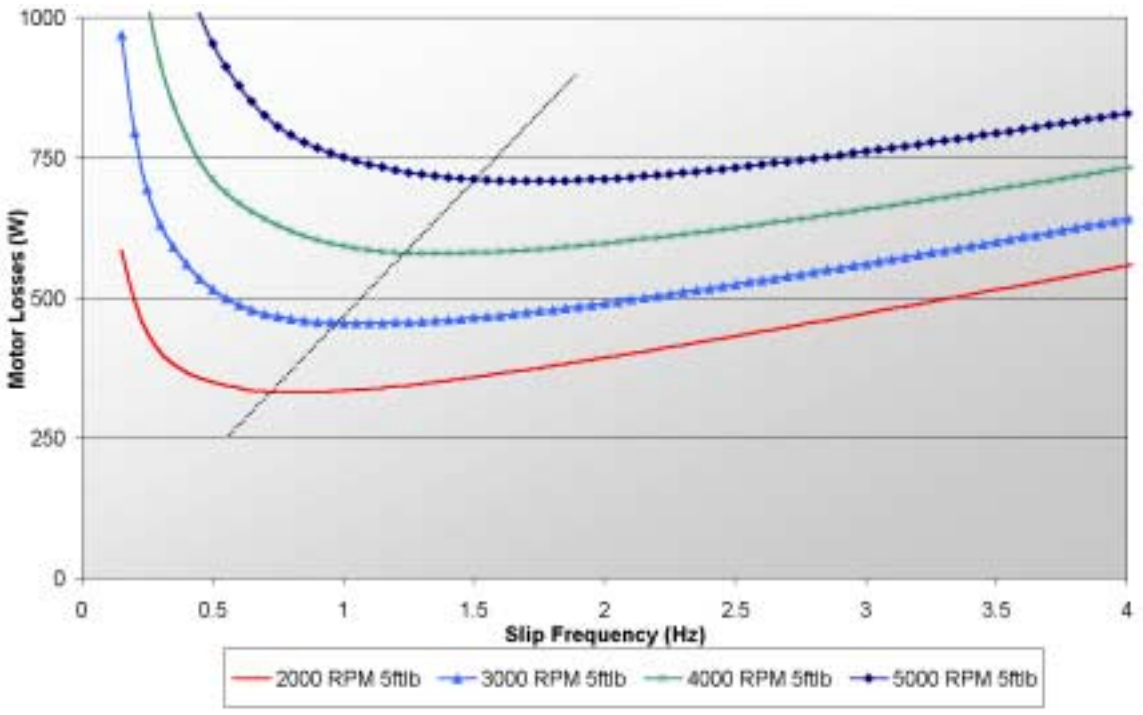

Figure 14 Motor Losses - 5ft-lb

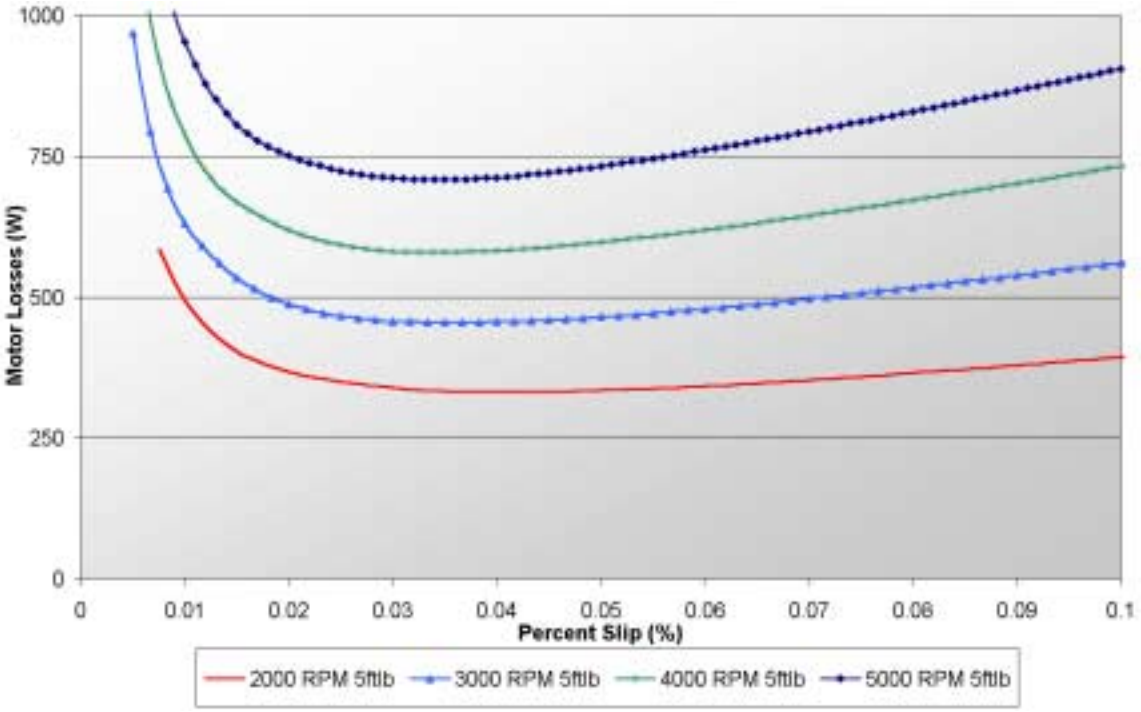

Figure 15 Motor Losses vs. Percent Slip - 5ft-lb

The next test to be run was looking at the minimum stator current required to generate a desired operating condition. When the maximum torque per ampere curves were plotted for a rotor speed of 3000rpm and a variety of torques, one can see a definite trend in the relationship between the slip frequency and the minimum stator current. The slip that gives the maximum torque per ampere increases as the shaft torque increases. This means that the curve minimums shown in Figure 16 are not slip independent as the minimums in Figure 13 were. At first glance, it might appear that this would make minimum stator current control a difficult and thus undesired alterative. However, stator current is a quantity that can be directly measured so the low point does not have to be predicted.

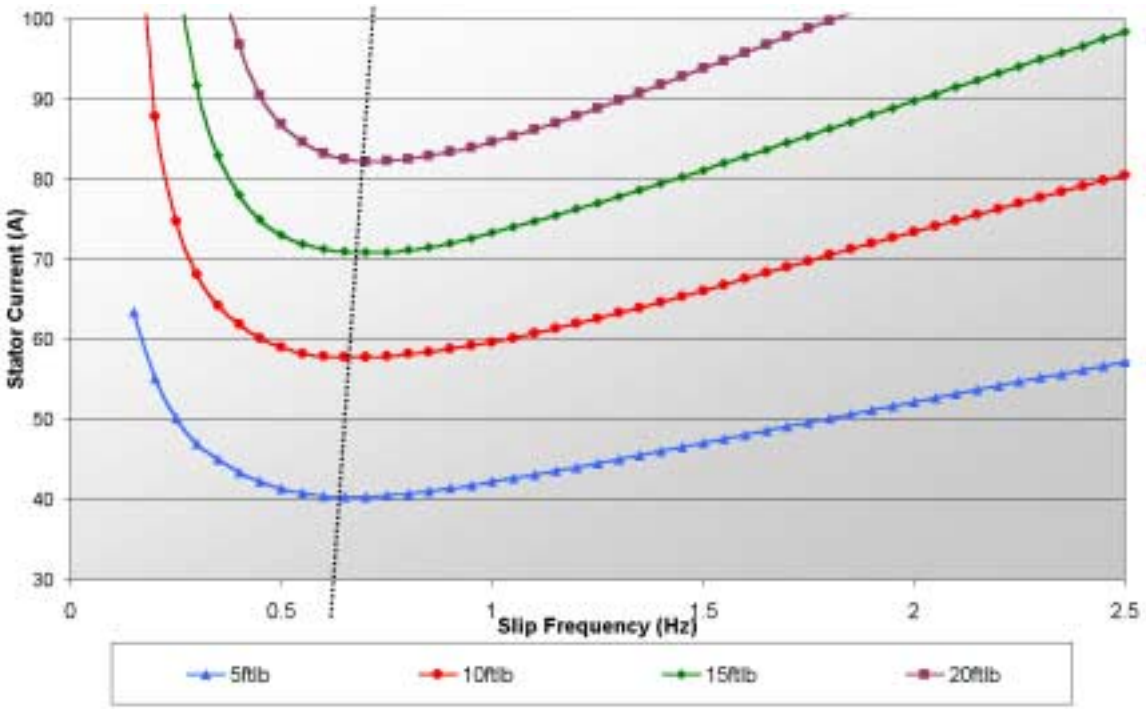

Figure 16 Maximum Torque per Ampere - 3000RPM

The slope of the dotted line connecting the minimum points in Figure 16 is a guide to the level of dependence of minimum stator current on slip frequency. Figure 17 takes this analysis to the next step by showing another set of curves for a higher shaft speed. It is quite clear by looking at the slopes of the lines passing through the curve minimas that dependence increases with speed. This is demonstrated because the change in slip frequency for between different torque levels increases as the rotor speed increases from 3000RPM to 5000RPM.

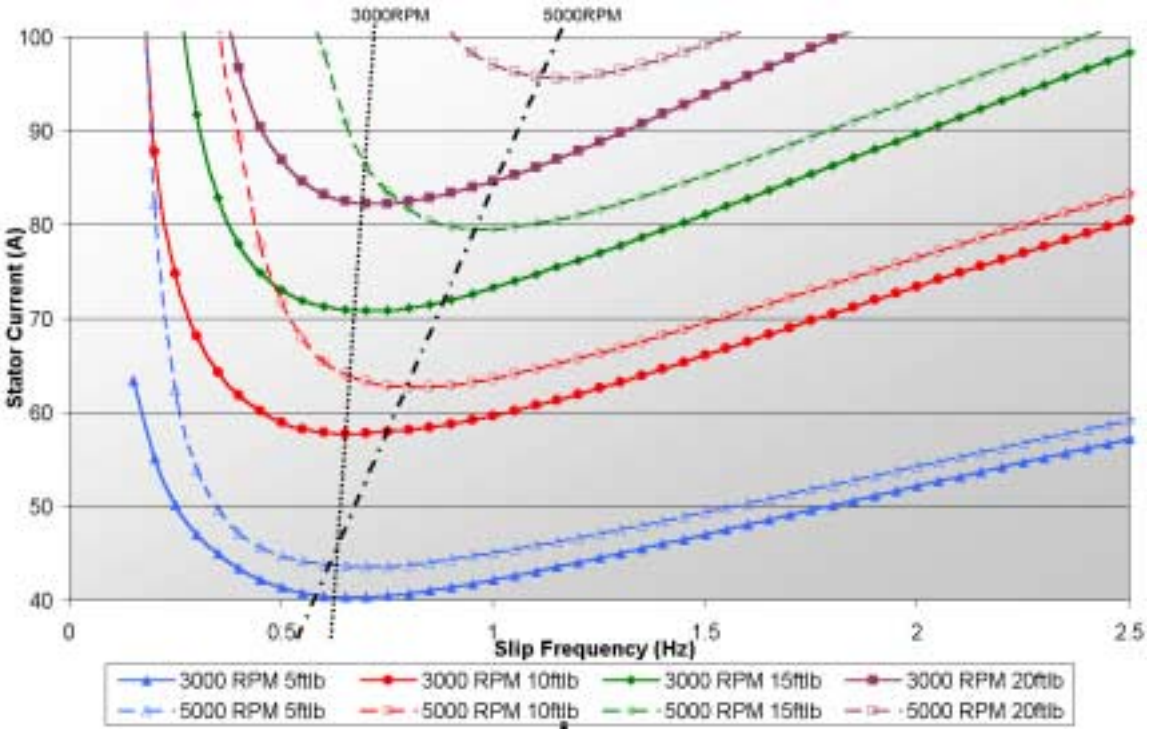

Figure 17 Maximum Torque per Ampere - Two Rotor Speeds

By running multiple rotor speeds for a specified torque level, a clearer picture of the relationship with slip emerges. The relationship is not linear as with the minimum motor losses. The nonlinear nature of the relationship causes a larger difference in slip frequency to be required for each incremental increase in speed. This is shown in Figure 18. It is also evident from looking at the graph that as the torque is increased the effect becomes more prominent. Obviously, at 10 ft-lb of torque, the slip/current relationship is much more nonlinear than at 5 ft-lb.

Another way of looking at the data is to take the data and re-plot the speed dependence versus the fractional slip rather than the slip in frequency. This is the same technique as shown in Figure 15 for the minimum power analysis. Figure 18 shows that unlike the former analysis of Figure 15, the curve minimums are nowhere close to occurring at the same percent slip. This re-emphasizes the nonlinear nature of the relationship.

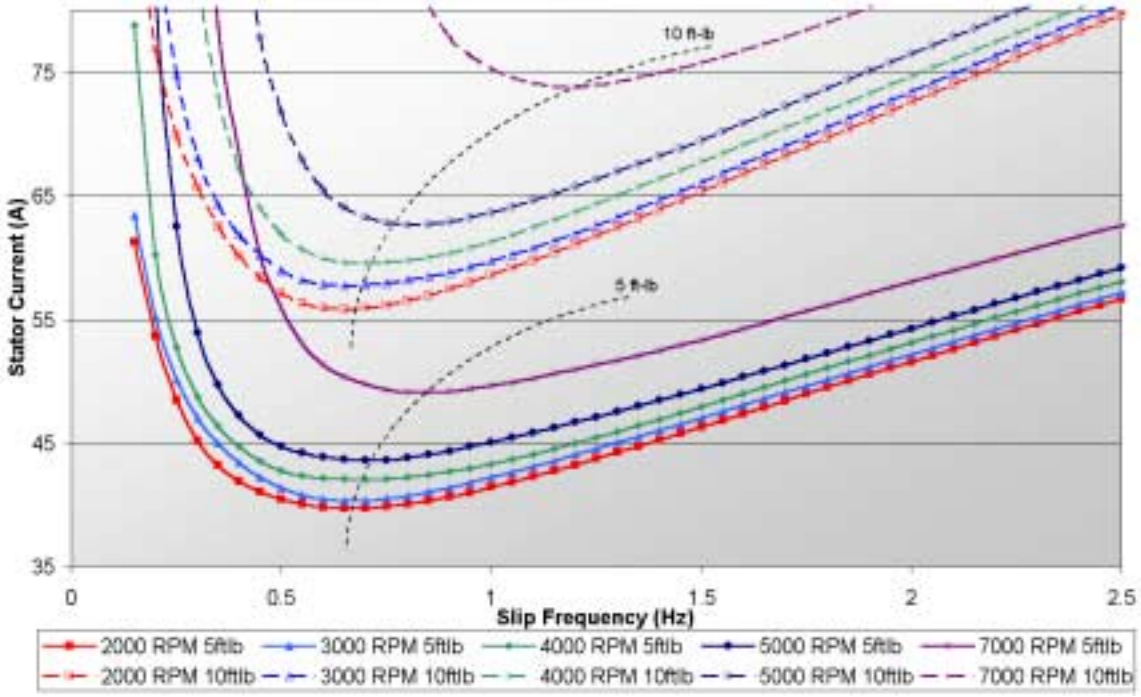

Figure 18 Maximum Torque per Ampere for Various Torque Speed Combinations

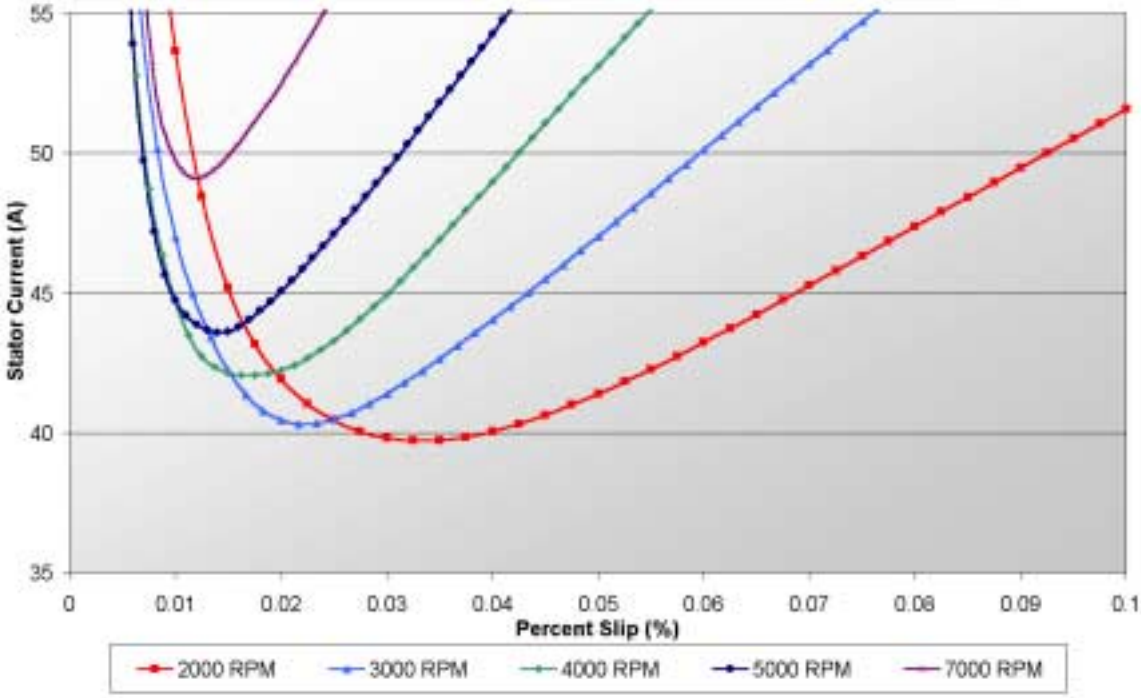

Figure 19 Maximum Torque per Ampere vs Percent Slip

Another interesting point involves the relationship between the rotor current and magnetizing current at the point where the stator current is minimum. Figure 20 shows that over a given slip range the maximum torque per ampere occurs at the point at which the magnetizing and rotor currents are equal. It is important to note, however that this does not always occurs. This convenient relationship seems to only work in low speed ranges. The simulated operating conditions in Figure 20 are for a rotor spinning at 3000RPM and generating five foot-pounds of torque. Figure 21 shows that the general rule still applies when the torque is increased, in this case to 25ft-lb. However, the rule does not apply when the speed is increased. Figure 22 shows that when the shaft speed is increased to 10,000RPM the maximum torque per amp no longer occurs where I_m and I_r are equal. In fact, about 10 amps separate the two currents when the stator current reaches its minimum. The reason that there is such a greater dependence on speed is that the core loss varies with frequency to the 1.5 power and is also a non-linear function of voltage. These nonlinearities dictate that the magnetizing impedance changes faster than the rotor impedance, which means that the two currents are equal at a different spot.

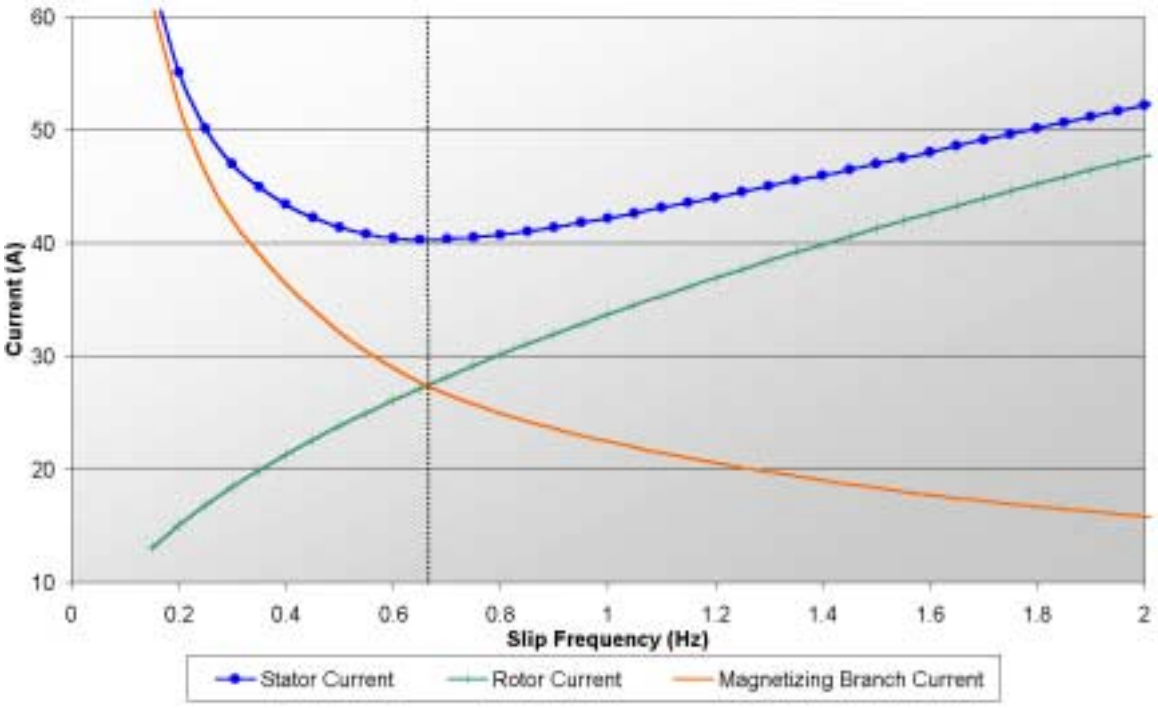

Figure 20 Various Motor Currents - 3000RPM 5ft-lb

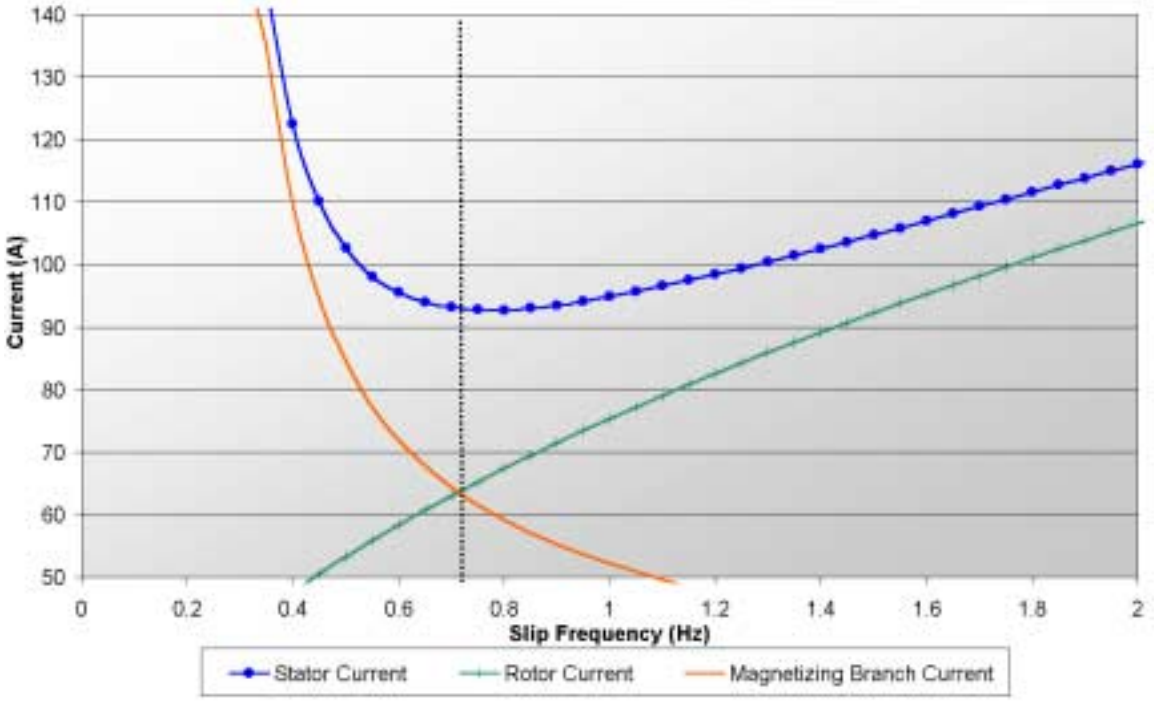

Figure 21 Various Motor Currents - 3000RPM 25ft-lb

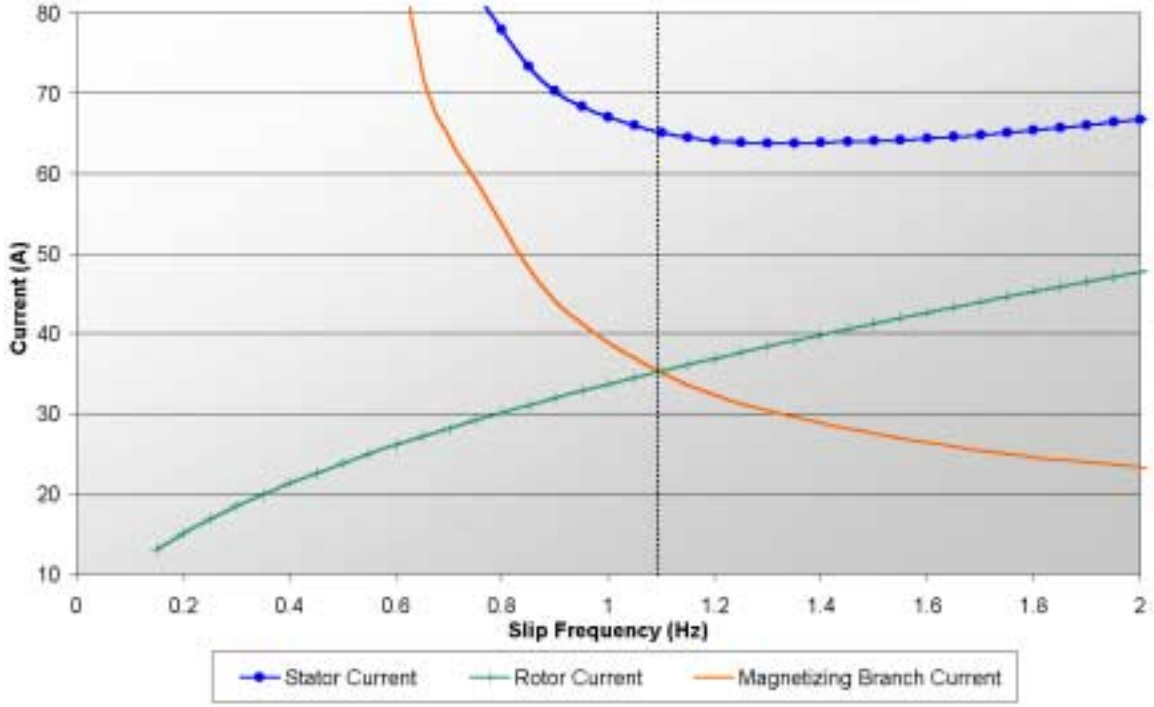

Figure 22 Various Motor Currents - 10000RPM 5ft-lb

2.5. Summary

This chapter described the method of modeling an induction motor for a traction drive. The model used in this work was a simple scalar electrical circuit model that has been used in past and is accepted as a standard, industry wide. This model was used to simulate different operating conditions using motor parameters found as described in a later chapter. A method was described for taking a given operating speed and torque and then working back through the model to obtain the stator current and motor performance data. Then the simulation program in Mathcad was based on the model and used to demonstrate several different operating conditions. The results were displayed on various graphs and conclusions drawn from the results. First, it was shown that the slip at which the motor runs most efficiently is not the same as the slip where the stator current is minimum. Next, it was demonstrated that the minimum power occurs at the same slip regardless of torque but that the slip for maximum efficiency does change with speed. Unlike the maximum efficiency point, the slip at which the maximum torque per ampere was shown to vary with both torque and speed. Finally, it was demonstrated that the stator current reaches a minimum at the same point that the magnetizing current equals the rotor current only under low torque and low speed. At higher speeds, the minimum stator current does not correspond to an equal current sharing between the two branches or the circuit model.

Chapter 3: Experimental Setup

3.1. Introduction

This chapter deals with the method and setup of the experiment that was used to demonstrate the points simulated in chapter two. First, it describes the motor that was used and its specifications. The motor was specifically designed as an induction motor for a traction drive application. Next, the specifications and design points for the inverter are presented and explained. The inverter was designed as an integrated unit in order to minimize losses and parasitic effects. The special techniques used in the construction of the inverter are described. Finally, the experimental method used throughout the tests is described in detail. A uniform testing procedure was developed so that the data was collected under uniform conditions so that results could be trusted. All the points above are summarized in the final section of the chapter.

3.2. Hardware Setup

The previously described concepts were validated in the lab using a custom built motor and inverter. The inverter was designed and built in house, while the motor was designed by VPT and built by General Electric. The motor and inverter will later be integrated in to a single traction drive unit as shown in Figure 23. This section describes the construction and integration of the test setup. The motor is described first and then a detailed examination of the inverter is given.

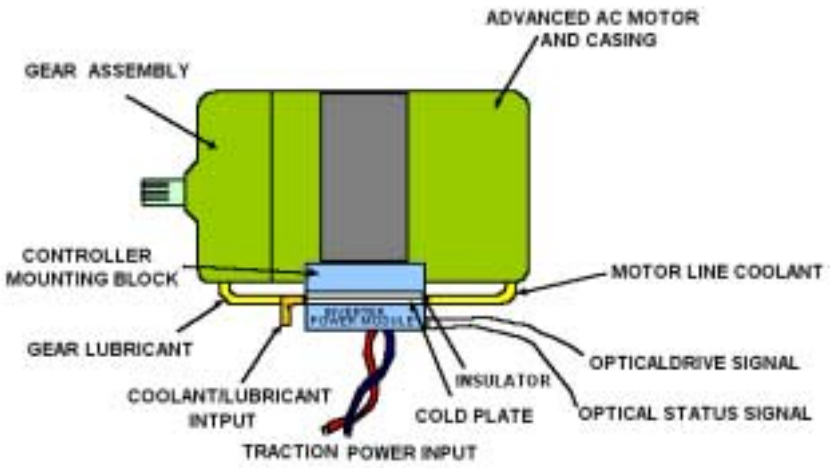

Figure 23 Motor/Inverter Unit Assembly Drawing

3.2.1 Traction Drive Motor

The motor used in this work was purposely designed to be used as the main drive motor in an electric vehicle. A traction drive application has special characteristics which become evident due to the nature in which the motor must start a large mass moving from dead stop and then maintain that mass at a high speed and be able to handle rapid acceleration and deceleration. Because the motor must start the heavy vehicle from a standstill, it must be able to generate high torque levels. It must also be able to maintain the torque during acceleration. However, after generating high power levels during acceleration the motor must be able to level out and drive the vehicle at higher speeds but lower torques. The motor must also be able to do the two items mentioned above with a high degree of efficiency.

The motor used in this work was a first prototype of the motor that will be used in the final traction drive package that must be delivered at the culmination of the project. The motor is a 60-Frame motor. The outside diameter of the stator is 7.36” and the stator stack up is 7” high. The weight of the stator comes in at 60lbs. The outside diameter of the rotor is 3.94” and the rotor weighs 17.5lbs. The prototype of this motor is shown in Figure 24. The motor shown is a 60-frame motor that will finally be housed in a 180-frame in order to build off current designs and allow room for cooling and inverter integration. The motor used in the previous iteration of the research effort was also in a

180-frame housing. However, the rotor and stator combination were classified as an 80-frame motor. That means that the old motor was larger with an outer diameter of 8.75" and a stack length of 7.5". The reason that the new motor could be made smaller hinges on a rule of thumb called Esson's Rule. This guideline states that the power a motor can produce is proportional to the speed times the motor volume. Therefore, if the size is reduced the speed must be increased. For this reason, the new motor has a maximum speed of 20,000rpm while the old design was limited to 15,000rpm. In other words, the final product will produce the same power as the old design by running 30% faster.

Care was taken in the design for the motor to be able to run efficiently at higher speeds in order to reduce the size and get extra benefit by reducing the weight. In order to build this motor using a 180-frame housing, a tube will be driven into the housing to serve as a spacer and to take up any slack. Next, the stator stack will be slid into the tube mounted in the housing and the motor assembly is completed.

Figure 24 Prototype Induction Motor for Traction Drive

3.2.1 Integrated Inverter Design

In developing this project it was determined that an inverter would need to be built that could handle the high current levels during acceleration and regeneration and yet be efficient at low power. As detailed earlier, a traction motor drive system spends most of its time at low torque, which corresponds to lower power levels transmitted through the inverter. However, during start-up and braking the inverter can experience high power levels. While this period may not last more than 30 seconds, for power electronics systems, this can be considered steady, state both electrically and to some extent, thermally. For thermal reasons as well EMI and efficiency, much care must be taken when designing the inverter. There were several areas where this unit was designed specifically to minimize an adverse effect. Some of these points are covered in more detail in the following discussion.

First, a generalized block diagram of the motor drive is shown in Figure 25. This illustrates the fact that the DSP and control logic was virtually isolated from the high power inverter by using optical fiber. This allows the control to be placed several meters away and be completely unaffected by switching transients that may occur on the high power side. The block for the IGBT inverter is expanded as a schematic in Figure 26.

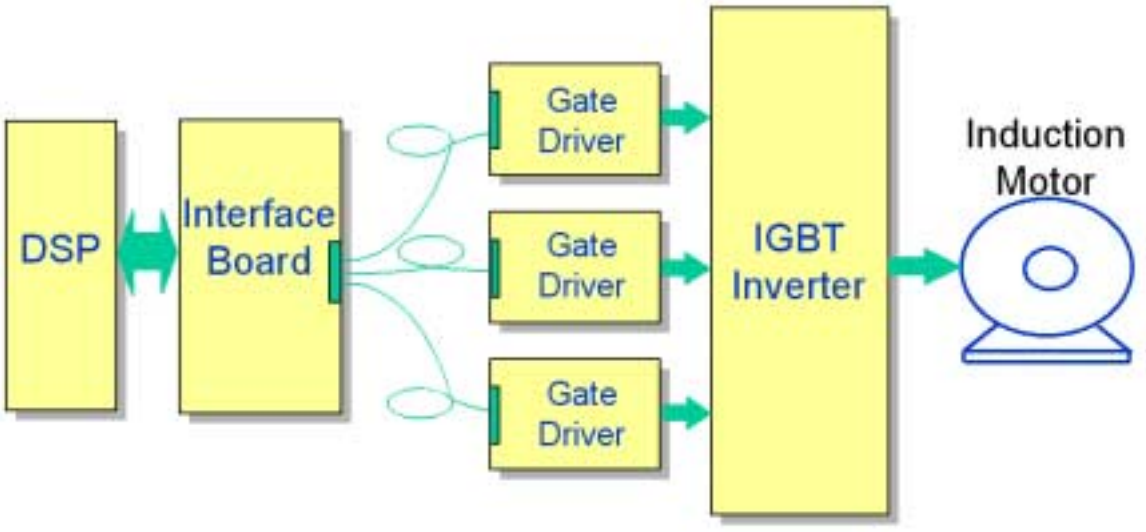

Figure 25 Experimental Setup Block Diagram

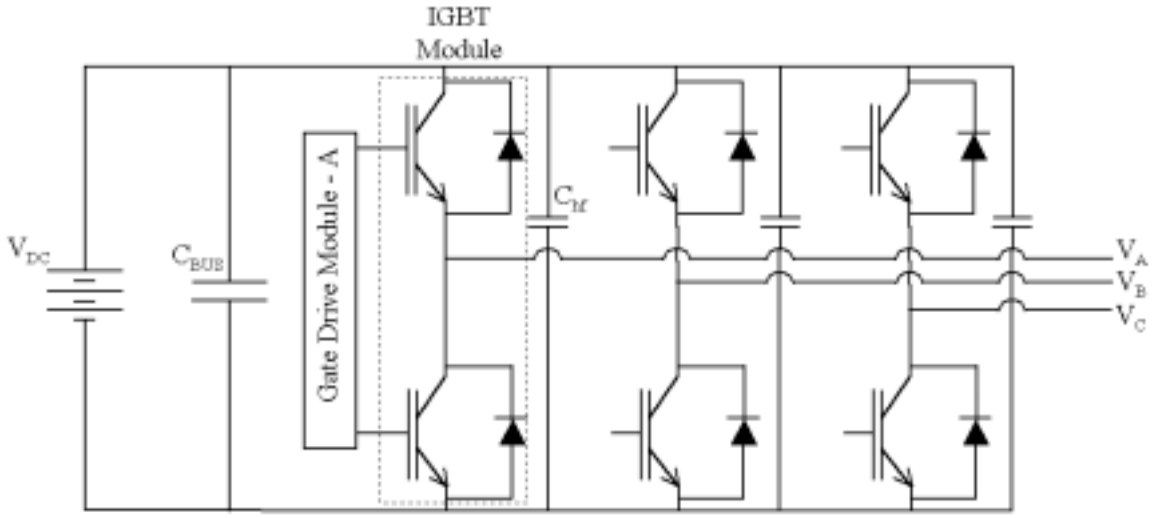

Figure 26 Motor Drive Inverter Power Circuit Schematic

The inverter used in this drive was a three phase IGBT based inverter. It was designed to use half bridge modules for current carrying capability. The inverter was designed for 75kW with a maximum DC bus voltage of 300V and a maximum current of 300A. The modules used for the test were Semikron model SKM 300GB 124D. The connections between the modules were made via a specially constructed busbar. Rather than use typical laminated copper sheets, a PCB approach was used. Because of the high current requirements, the board shown in Figure 27 has 15-ounce copper, which means that the copper is 21 mils thick. This is considerably thicker than a typical signal board, which uses copper that is 1.4 mils thick. The board shown below has four layers. The two internal layers are used to carry signals from the gate drive modules to the control pins on the IGBT modules. These traces were routed in such a way as to minimize the loop area between the gate and source of each IGBT device. Also included on the board was a common mode filter, which was included to aid in the suppression of conducted EMI transmission. The choke used in the filter was a single turn inductor that used an E-I core set clamped into slots in the PCB as another level of integration.

Figure 27 Inverter PCB Integrated BusBar

The gate drivers used in this test setup are integrated modules that were developed to pack the most functions in a very limited space. A block diagram of the gate drive circuit is shown in Figure 28. The gate drives receive an input PWM signal from the control board via an optical fiber. This signal is converted to electrical and then adjusted to go between +15 and –5 volts to properly bias the device when turning in off and on. A common power supply serves all the gate drives and this is isolated with a small flyback isolating DC-DC converter. This allows each device to be properly referenced to the device it is controlling in order to turn it off and on. The gate drivers also provide fault protection by sensing the desaturation of the power device and sending an appropriate signal back to the DSP to turn off the inverter. The gate driver circuit itself automatically turns off the offending device very quickly and in this way protects the device from possible short circuits that would otherwise destroy the IGBT.

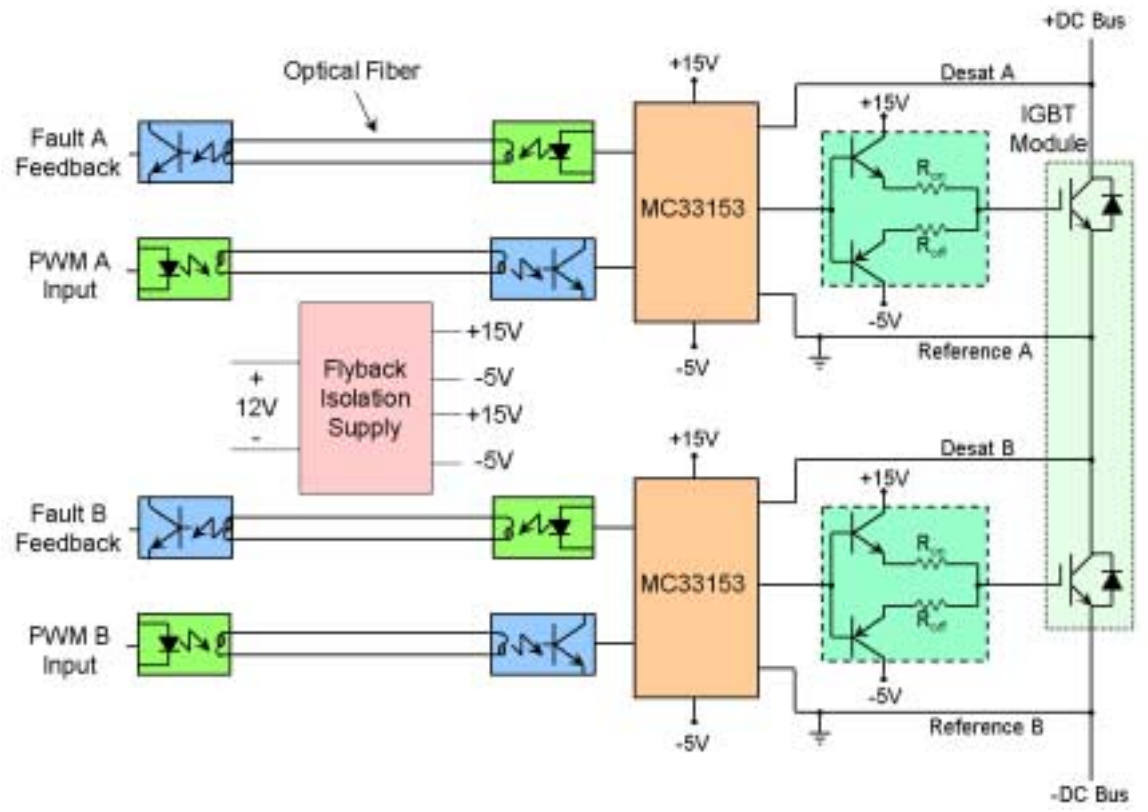

Figure 28 Block Diagram of Gate Drive Circuit

The gate driver described above is shown in its physical form in Figure 29. The module serves a half-bridge IGBT module and provides isolation between the gate signals.

Figure 29 Gate Drive Module

Another precaution that was taken was to add high frequency capacitors to the DC bus. Working closely with Electronics Concepts, a DC bus capacitor was developed that would handle high RMS current as well as meet specific height requirements. The large capacitor was applied directly across the bus to handle the majority of the ripple current. The length of copper between the capacitor and the IGBTs is effectively an inductance

and the larger the inductance, the larger the L*di/dt, resulting in higher transient voltages. This can cause undue stress on the switching devices and lead to excess losses. For this reason, smaller, low inductance high frequency capacitors from Electronic Concepts were placed directly across the DC bus terminals on each IGBT module. This process virtually eliminates the transient overshoot voltages. The large capacitors from Electronic Concepts are listed as UP9 200uF and 500Vdc. The small caps are known as MP8 2uF 800Vdc.

Figure 30 DC Link and High Frequency Bus Capacitors

The integration of the high frequency capacitors directly across the DC bus at each module and elimination of excess parasitic inductance by utilizing a PCB busbar helped the performance of the inverter unit and greatly reduced the voltage overshoot seen by the devices. This means that a device with a lower rating can be used which leads to lower cost and lower losses. Figure 31 shows a drastic improvement over traditional laminated busbar approach. When the two busbars were tested under similar circumstances, the integrated PCB approach reduced the overshoot from 45% to 8%. This is a very significant decrease and while some of the performance can be attributed to better capacitors, Figure 32 shows that even without a bus capacitor the devices only experienced a maximum of 16% overshoot. This is still much lower than the laminated bus approach result. The data collected on voltage overshoot was generated using pulse testing on a single device.

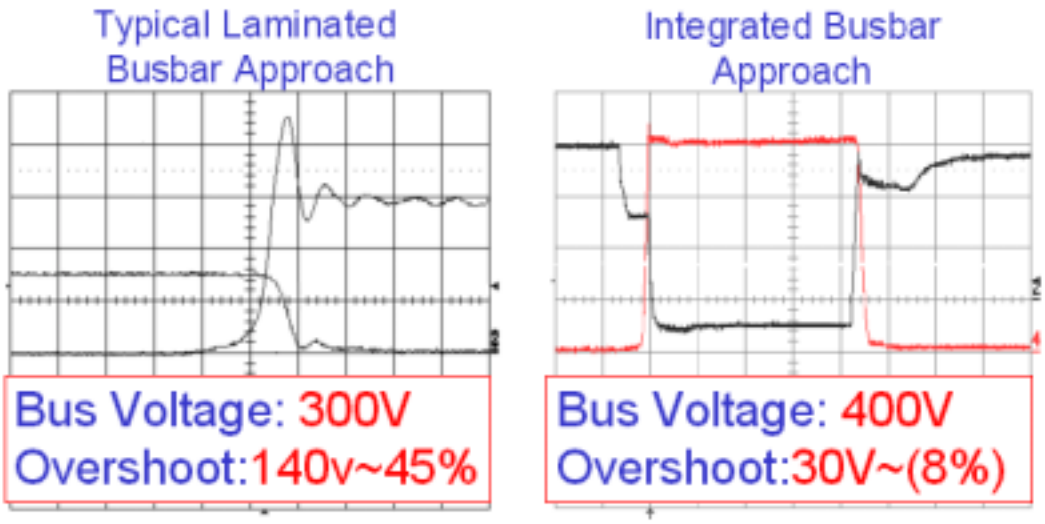

Figure 31 Comparison of Voltage Overshoot

Bus Voltage	No Cap		2 Cornell Dublier Caps (2u)		1 Electronic Concepts Cap (2u)	
	Value(V)	Percentage(%)	Value(V)	Percentage(%)	Value(V)	Percentage(%)
100	16	16	12	12	10	10
400	56	14	38	9.5	30	7.5

Figure 32 Table of Voltage Overshoot Examples

Figure 33 Integrated Gate Drivers and Capacitors

In order to eliminate excess thermal losses the IGBT modules were soldered to the base plate rather than bolted. This has been shown to greatly improve the heat transfer away from the IGBT die in the module.

Figure 34 IGBT Modules Soldered to Base Plate

In the assembly the base plate was then bolted down to a heatsink and all the control wires and optical cables were attached. Figure 35 shows the assembled inverter with capacitors and gate drivers attached.

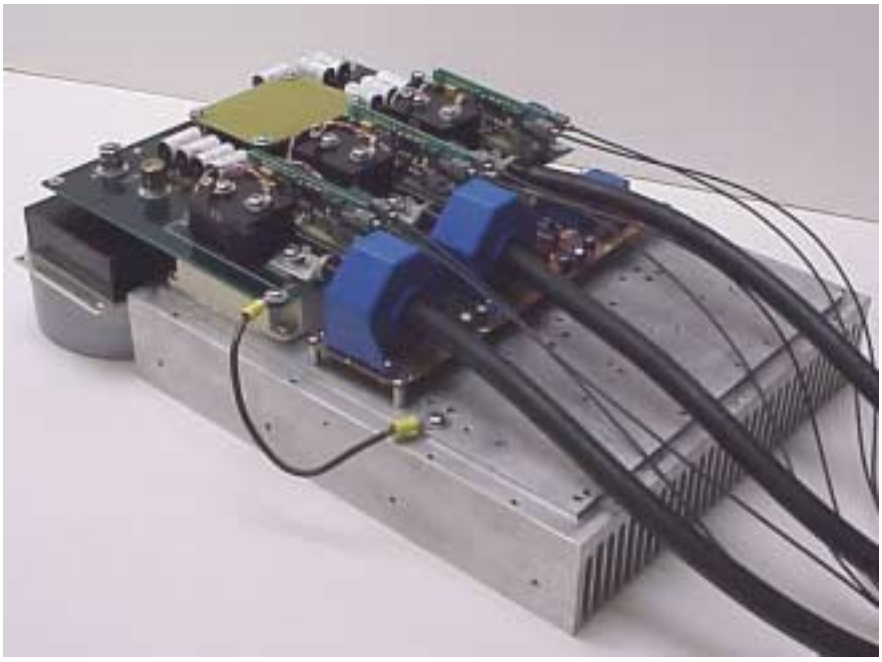

Figure 35 Inverter Mounted to Heat Sink with Fiber Optic Control Lines

Figure 36 shows the test setup as it was realized in the lab with the dynamometer and all the sensors attached. The Dynamometer is a Yaskawa Varispeed 626VM3. The torque sensor and meter are Himmelstein brand.

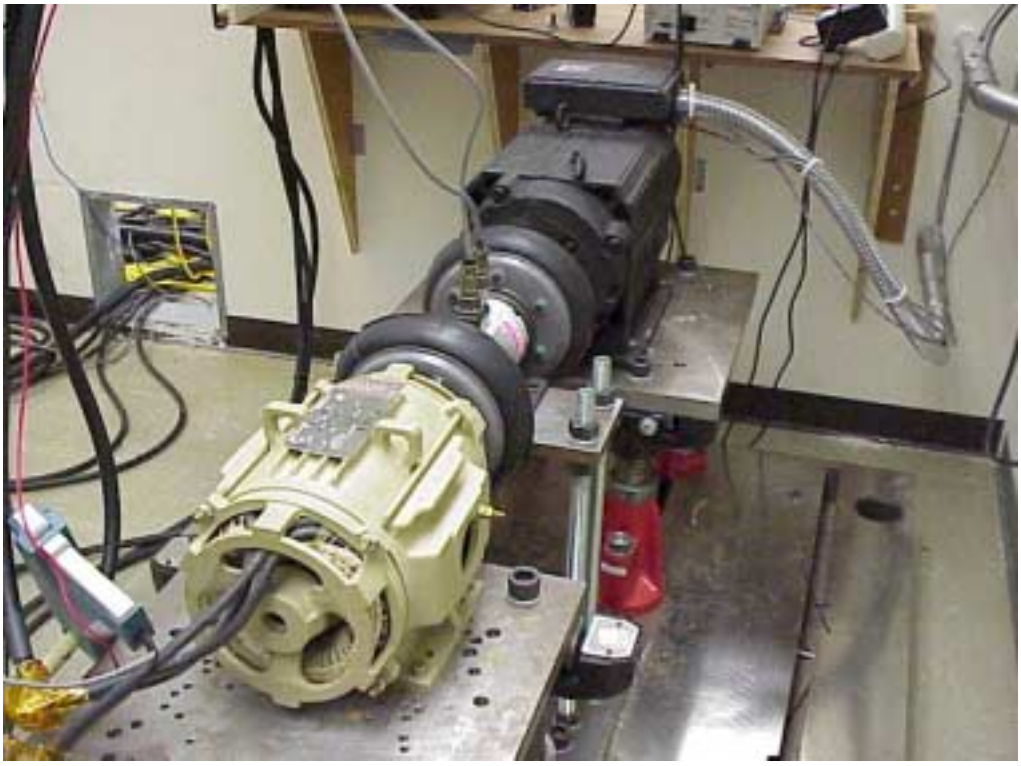

Figure 36 Traction Motor Drive Connected to Dynamometer

3.3. Experimental Method

In order to fully characterize a motor drive at low torque or low speed the experiment must be constructed in such a way that the incremental change in variables must be much smaller than the absolute value of the variable. This dictates that measurement devices be accurate enough to reliably display the changes that occur in various quantities. It also demands that controlling hardware be able to initiate changes in independent variables in small enough increments so as to be able to track trends in performance and provide enough points to be meaningful. In the ideal case the rotor speed would be fixed and the inverter output frequency would be varied. However, in this case the DSP program did not have the resolution to set the electrical frequency in small enough increments so the synchronous speed was held constant and the rotor speed was changed to vary slip. It was also found that rather than dialing the modulation index into the controller via a potentiometer, it was more precise to hold the modulation index

constant and vary the inverter output voltage by adjusting the DC bus voltage. The motor drive / dynamometer combination was run in open loop so that all variables could be monitored and changed independently. That being said, in order to obtain high quality, believable results, a strict detailed test protocol had to be developed and followed so that results from different times and conditions could be faithfully compared. That testing procedure is given below.

The first step was to set the output frequency of the inverter using the admc401 in order to get the no load rotor speed as close to the nominal target value as possible. Next, the line-to-line voltage would be set to an acceptable level by adjusting the DC bus of the inverter. At this point the rotor speed is regulated down using the dynamometer controller to produce a slip frequency between the rotor speed and inverter output frequency. The torque was monitored and the slip was increased until the torque was at the desired level. The setup was run under this condition until the system reached thermal steady state. After the system finished its thermal transient, the rotor speed and motor terminal voltage were adjusted in order to acquire a large slip. This occurs at a lower voltage level while a small slip occurs at higher voltages. The data collection then began by recording the rotor speed, line-to-line voltage, phase current, DC bus voltage and current and the real power delivered to the motor. Between each data point the voltage was increased and then the rotor speed was increased (which in fact lowered the slip) in order to maintain the desired torque. The voltage was increased in essentially one-volt increments, which entailed collecting a good many points in order to cover a slip frequency range from around 3Hz down to less than 0.5Hz. This process was repeated for each speed/torque combination.

3.4. Summary

This chapter outlined the specifications and design criteria used in building up the hardware test set. The motor designed for traction drive applications was described and specifications were given. The majority of the chapter dealt with the design and construction of an IGBT based inverter that was specifically designed to eliminate

parasitics and improve performance. The method for isolating the control from the high power circuit was described. The gate drivers that were used to isolate each the control signal going to each device were detailed. It was shown that the inclusion of high frequency capacitors across the DC bus made a marked improvement in the elimination of voltage ripple. The improvement in voltage ripple due to the PCB based busbar was also examined. The method behind the layout of the PCB was also described and the assembly process for the motor drive was described. The design and layout of the inverter and drive unit can have just as much effect on the performance of the system as the devices that are chosen and the tasks should not be ignored if an effective system is being designed.

Chapter 4: Analysis of Experimental Results

4.1. Introduction

After analyzing the simulation results and determining the best experimental procedure to follow, the motor was connected to the dynamometer test set and the inverter was connected to the motor. The system was then started under no-load conditions in order to verify proper operation and fault protection circuitry. This chapter presents the results from the hardware tests. The results showing each critical issue are plotted and the important points are emphasized and highlighted. Finally, the experimental results are compared with the simulation results and the key points are analyzed.

4.2. No Load / Locked Rotor Tests

Some of the first data that was taken on the motor was to characterize the motor parameters such as rotor and magnetizing impedances. The tests that were used were standard no-load and locked rotor tests. The test was run at 60Hz which is the common test point in the industry and the design data was developed at that frequency. The tests were run for a couple reasons. First, they were carried out in order to verify that the motor did indeed meet the design criteria. Second, data needed to be collected so that a look up table could be built in to the simulation program that accurately represented the real machine. The motor was run under locked rotor in order to determine the rotor impedances as referred to the stator. The no load test gives the magnetizing branch information. This is very critical because it varies with applied voltage and so instead of

a single number an entire table is generated. In this case, the motor was run at 60Hz over the entire voltage range that the motor would be subjected to and the data was collected. Figure 37 shows that the results that were obtained matched the design data very well.

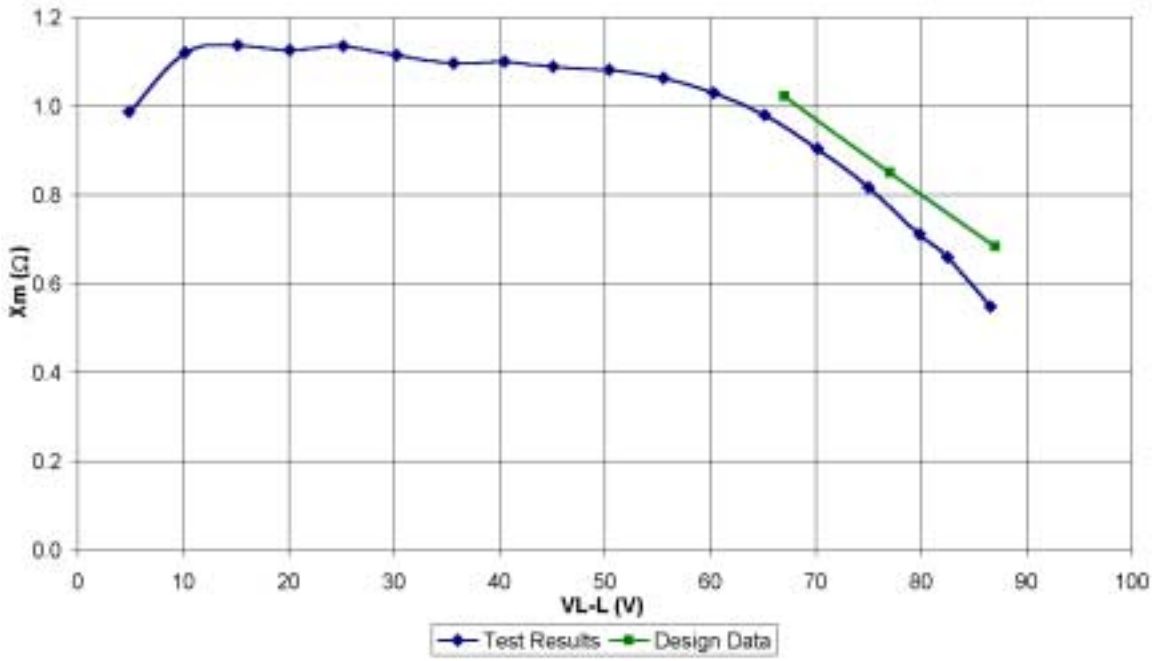

Figure 37 Magnetizing Impedance vs Motor Voltage

4.3. Hardware Test Results under Varying Conditions

After setting up the hardware test set and verifying the operational viability of the experimental plan, the motor drive was run under a variety of conditions to obtain a variety of data points centered around the torque and speed that it was determined a traction drive would spend the majority of its time. The upper limit of the test was limited by the power supply and cooling capabilities built into the current hardware test setup. The tests were run at roughly 1000 rpm intervals between 1000 and 4000 rpm. This is an approximation because the rotor speed was not fixed during the tests but typically, during a specific test the rotor speed would range within 200 rpm of the target speed. This speed range obviously leads to a slip ranging up to about 3Hz. From the simulations done earlier it had already been determined that the critical points would be captured by running the motor with slip frequencies less than 3Hz. As described above in

the section on experimental method, the voltage applied to the motor was varied in order to keep the output torque the same. As each test was run, the data was collected into a large spreadsheet. This allowed curves from different tests to be plotted easily on the same graph. All of the raw data that was collected is tabulated in Appendix A.

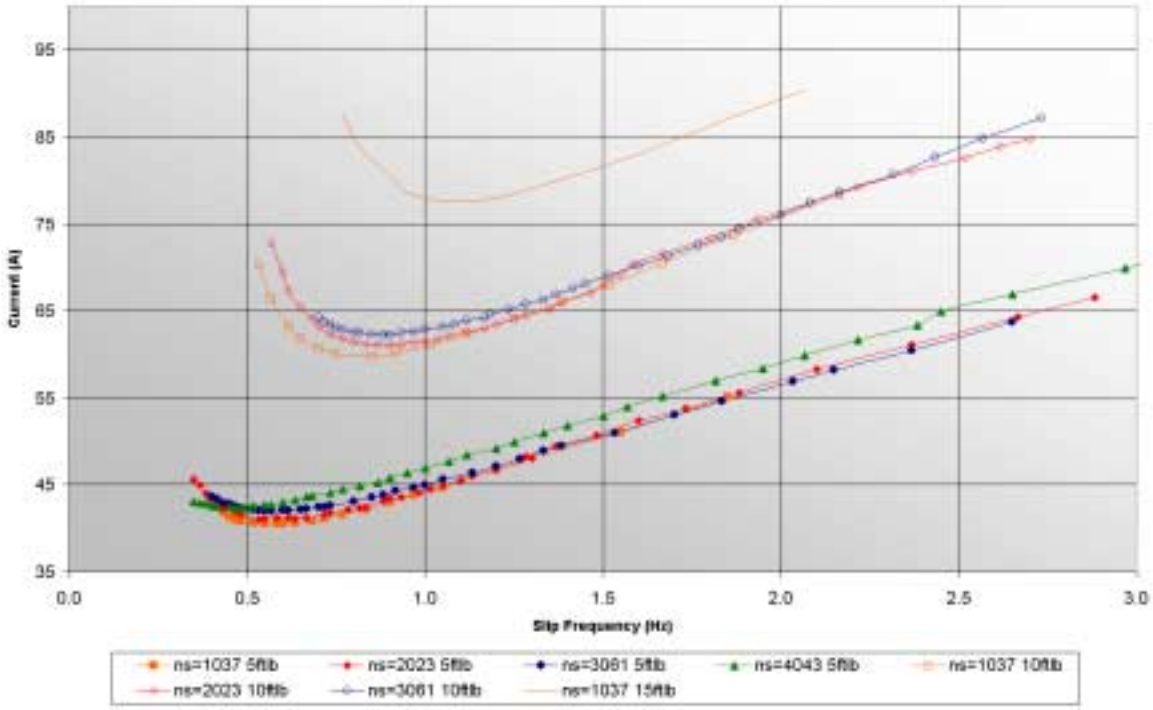

Figure 38 Maximum Torque per Ampere

Figure 38 shows the stator currents from all of the tests plotted against slip frequency. All of the curves demonstrate the local minimum around the ½ to 1Hz range. When this graph is compared to its simulation counterpart, Figure 18 a general agreement is noticed. Figure 38 shows the variance between the currents at a specific frequency than does Figure 18. This is because the rotor speed was held constant in the simulation while in the experiment the synchronous speed was held constant. However, the trend that as torque is increased the slip at which minimum current occurs also increases is still valid and is shown on both graphs.

The minimum motor loss curves for the different speeds at 5ft-lb are shown in Figure 40. The point at which maximum motor efficiency occurs is between 0.8 and 1Hz. It is also evident that just moving away from that minimum by a fractional Hertz can affect the power loss by tens of watts. The complimentary plot showing motor losses

for a variety of torques at a specific speed is shown in Figure 39. These plots correspond to simulation output shown in Figure 13 and Figure 14. An important observation is that Figure 39 does not show the independence of motor efficiency to torque that Figure 13 indicates. This is again a by-product of the difference between the experimental method and the simulation technique. This is addressed in the following section. Figure 40 shows that there is a dependence of motor efficiency on speed but the dependence is not shown to be the same degree that is represented in Figure 14. This is because in the simulation the rotor speed represented by each curve remains constant throughout the curve, which means that the output power is the same. The experimental curves are constantly varying the rotor speed and thus the output power so it is expected that the curves will not match exactly.

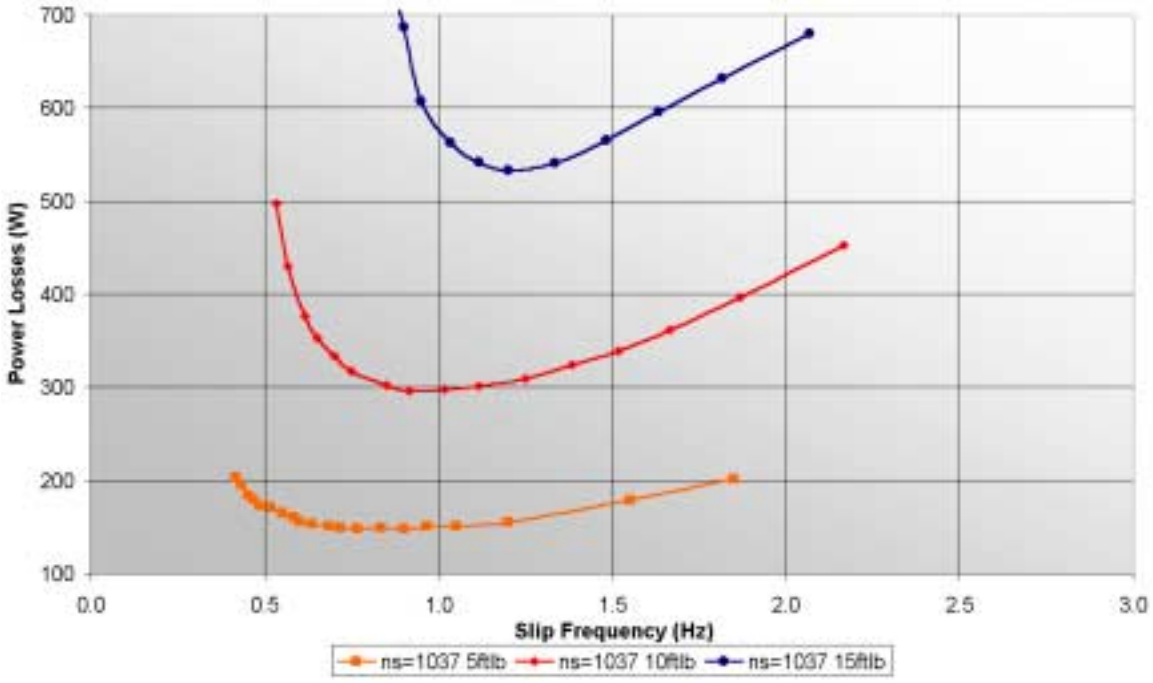

Figure 39 Motor Losses for Various Torques

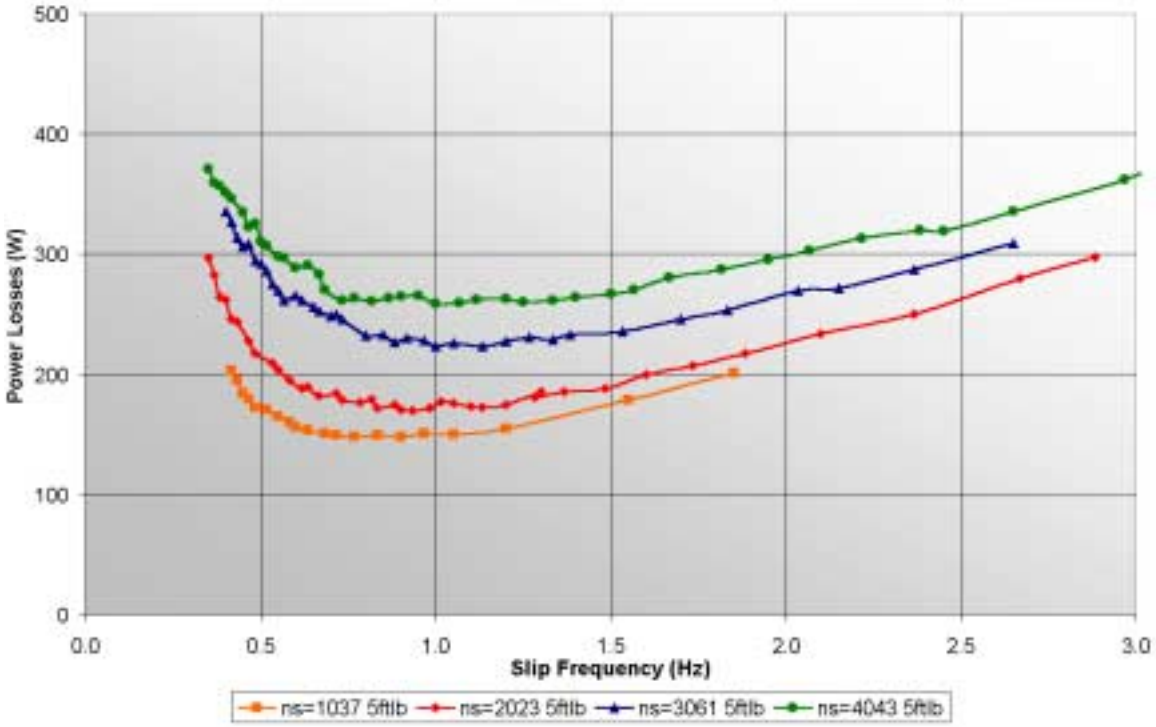

Figure 40 Motor Losses for Various Synchronous Speeds at 5ftlb

One point that was demonstrated through the experimental analysis but not through the simulation is that the system efficiency is also dependant on the slip frequency. Figure 41 takes data collected for both the motor efficiency and the stator current level at a torque of 5ft-lb when the inverter running at 51.01Hz and plots the data on the same graph. Because the power levels before and after the inverter were measured, the total system efficiency can be discerned by (4.1). This information is also plotted on Figure 41.

$$\eta_{sys} = \eta_{inv} * \eta_{motor}$$
$$\eta_{sys} = 1 - \frac{746 * T * n_{rotor}}{5252 * P_{in}} \quad \textbf{(4.1)}$$

The maximum system efficiency does not occur at the same slip frequency as the maximum motor efficiency. This is because there is more current passing through the motor at this point which means that the inverter has to switch higher currents which means that there are higher switching losses and higher thermal losses in the inverter. When the motor and inverter efficiencies are convoluted together as shown below the resulting peak is somewhere in between the point of lowest stator current and the point of

lowest motor losses. The results of the collected data indicate that the maximum system efficiency tends to be very close to the point of lowest stator current in the motor. Figure 41 and Figure 42 show that by running a traction drive at a slip frequency corresponding to maximum torque per ampere rather than at slip that generates the lowest losses in the motor will increase the system by one or two percentage points. That may not sound very significant, but one must realize that a pickup of 1.5 percent efficiency when the system is running at 85 percent to begin with is actually reducing the losses in the system by 10 percent. Another important point is that these numbers are shown for operating points at which the traction drive will spend the majority of its time. This means that a slight increase in efficiency when extended over a long period of time will generate a significant savings in energy costs.

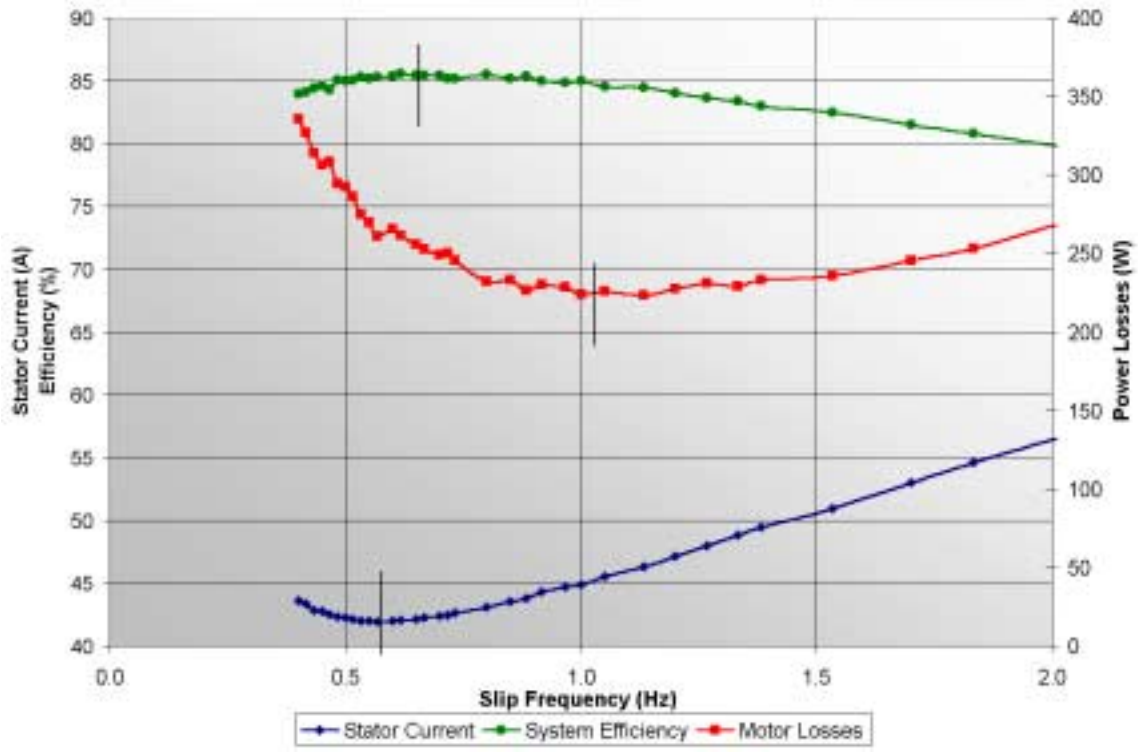

Figure 41 Maximum System Efficiency n_s= 3061 T=5ftlb

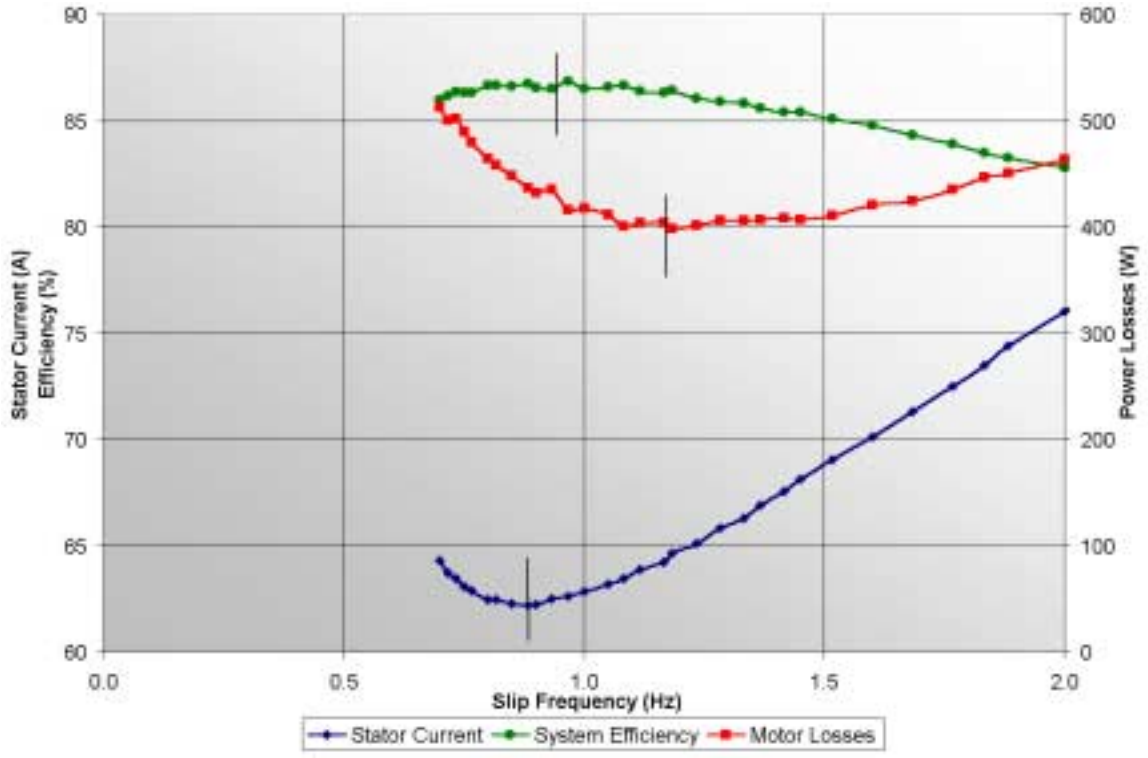

Figure 42 Maximum System Efficiency n_s= 3061 T=10ftlb

4.4. Simulation vs. Experiment

When the data in Figure 38 through Figure 42 is examined and compared to the simulation data in the previous chapter, several dissimilarities present themselves. At first, this was disconcerting since the simulation model was well thought out and did not seem to be flawed. It is also hard to argue with experimental data, especially when a strict plan of experiment was followed as described earlier. It turned out that, in fact, neither the experiment nor the simulation results were wrong. The cause for the graphs looking different is that the simulations shown earlier were run assuming a constant rotor speed. In order to generate slip in the simulation the electrical frequency was altered. In the experiment however, for reasons described earlier, the most precise results were obtained by holding the electrical frequency constant and varying the rotor speed to generate the slip. This made it difficult to verify the results and feel comfortable about any conclusions that were drawn. The solution was to alter the simulation routine such

that it mimicked the experiment and held the inverter frequency constant. The results of the experimental hardware setup were then used to verify this new simulation program. After the constant line-frequency simulation model was verified, then observations and conclusions made for the constant rotor speed model could be trusted with a high degree of comfort. The model was subjected to the exact criteria that were experienced in the hardware tests and the results were tabulated. Figure 43 shows the minimum power loss curves for a range of line frequencies. This graph can be directly compared to Figure 40. The results are very similar and lead to the conclusion that the model is in fact correct and can be trusted when making inferences and drawing conclusions from simulated data.

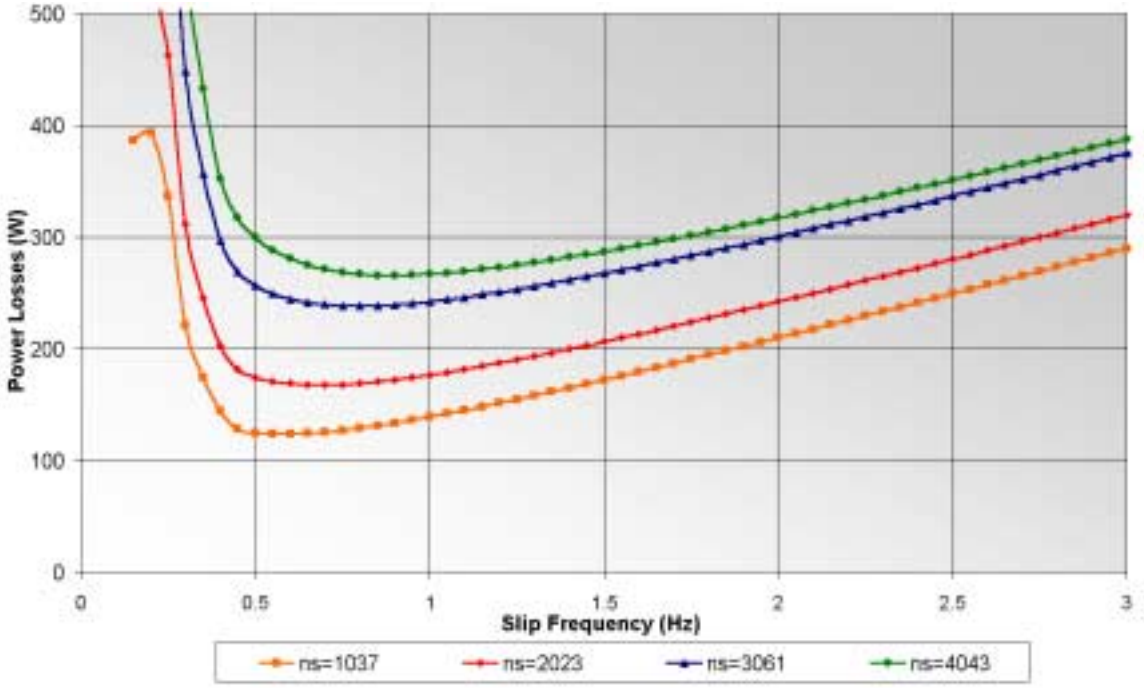

Figure 43 Motor Losses for Simulation with Fixed Line Frequency T=5ftlb

Figure 44 shows the results of the new model for the lowest stator current analysis and lowest power loss analysis for two torques at a line frequency of 51.01Hz. This graph can be compared directly to the results shown in Figure 41 and Figure 42. To simplify the comparison, Figure 45 shows the test data and simulated data for one torque/frequency combination on the same graph. While the results are not exact replicas, they show a high degree of correlation and again lead to a conclusion that the original model presented in Chapter 2 is in fact correct.

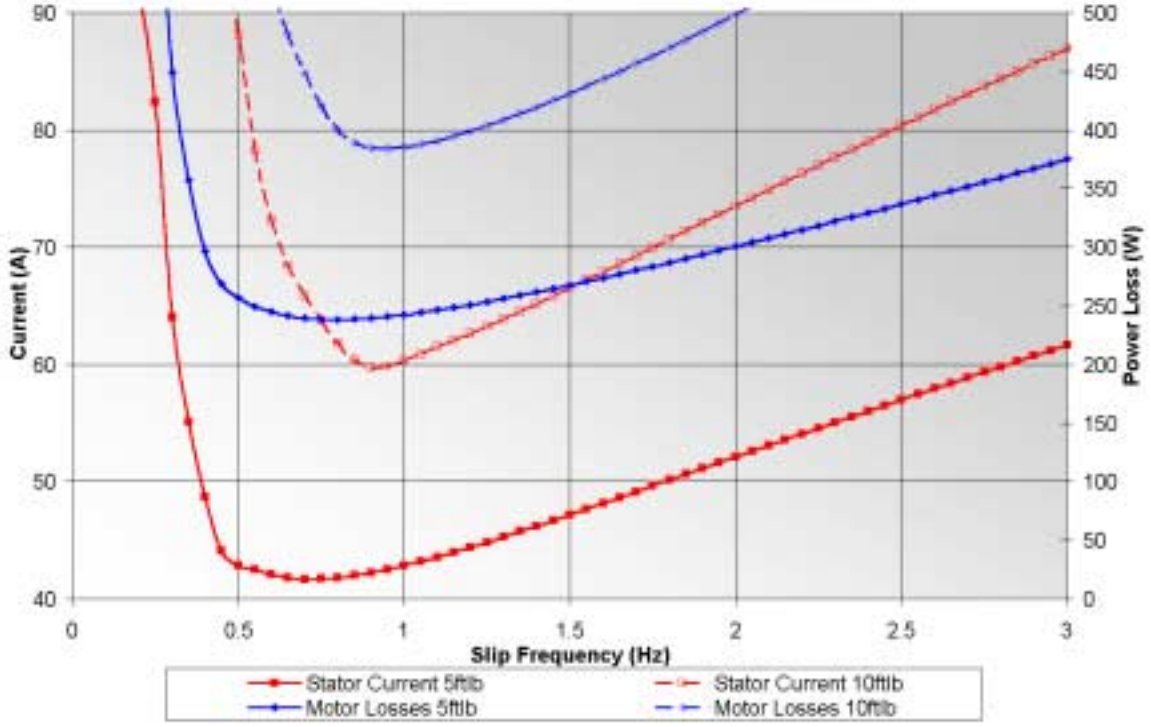

Figure 44 Simulations of Max T/A and Min Motor Losses n_s=3061

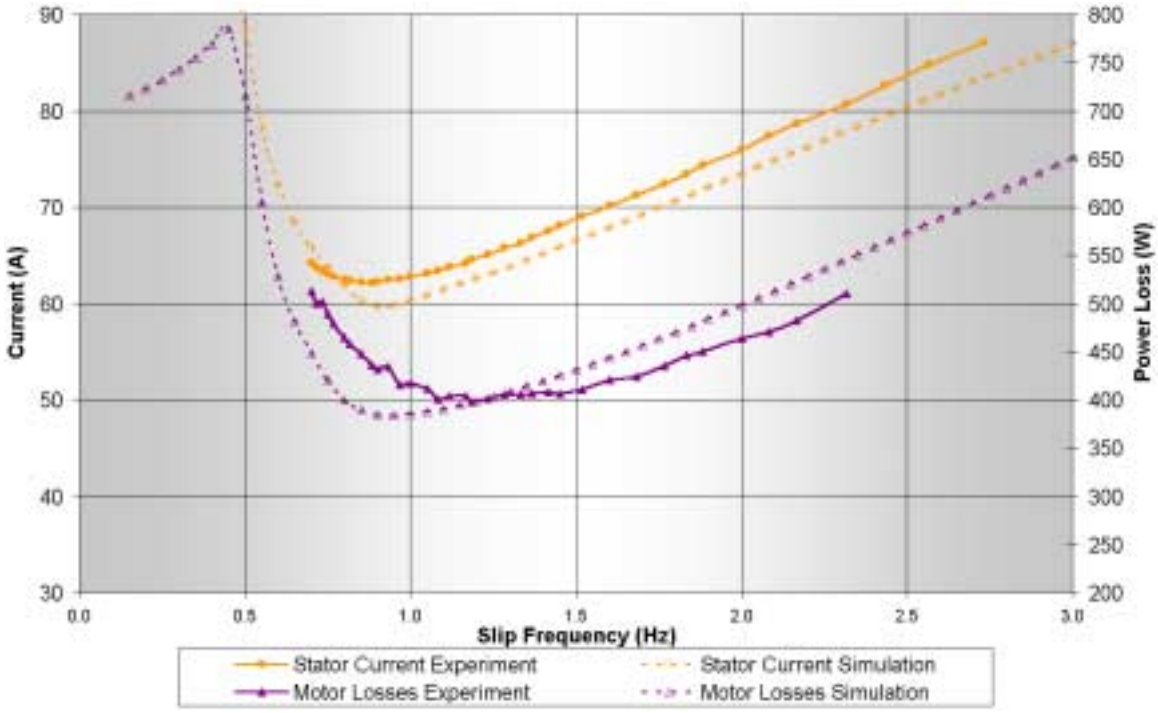

Figure 45 Comparison of Simulation and Experiment n_s=3061 T=10ftlb

4.5. Summary

The information presented above took several pages of data points collected over several different tests and combined them into a few revealing graphs. There are several salient points that were demonstrated and the differences between the experimental results and simulated were shown and discussed. The results were finally reconciled by altering the simulation program to mimic the experiment. This allowed conclusions drawn from both the simulation as well as the experiment to be trusted.

First, the motor was run under standard no load and locked rotor tests. The result was that the motor proved to have been built very close to the design specifications that were given to the motor manufacturer. Because of the altered simulation model and the comparisons showed that the model did indeed predict the operation of the motor, the conclusions that were made in Chapter 2 were validated. A new conclusion that was drawn strictly from the experimental data was that the motor drive as a system does not run optimally at the same point at which the motor runs most efficiently. The system seems to run most efficiently at a slip somewhere in between the slips that correspond to maximum torque per ampere and maximum motor efficiency. The data indicates that there is a pickup of a couple of efficiency points when the motor is run under a minimum stator current condition as opposed to a minimum motor loss condition.

Chapter 5: Conclusions and Future Work

5.1. Summary and Application of Results

This work took the scalar model of an induction motor and modeled it in an analytical math software. The model took the various nonlinear loss functions of the motor into account and scaled them appropriately with voltage and frequency. This model was then used to show the optimum slip frequency that corresponds to both the minimum loss in the motor as well as the minimum stator current needed to produce a certain torque speed combination. Conclusions were then drawn based on the analytical data that were later supported with experimental data. After completing the mathematical analysis, experiments were performed to verify the validity of the model. The results of the simulated model and the experiment were very close and comparisons between the two showed that the model did indeed predict the operation of the motor. This meant that the conclusions that were made in Chapter 2 were validated. The results listed below were demonstrated at various points throughout this work:

- The motor runs inefficiently under maximum torque per ampere
- The slip at which maximum efficiency occurs is constant for various torques, but changes with speed
- The slip at which maximum torque per ampere occurs, changes with both torque and speed
- Under low torque and speed, maximum torque per ampere occurs at the point the magnetizing current equals the rotor current.
- The motor drive system runs most efficiently at a slip in between the slips that correspond to maximum torque per ampere and maximum motor efficiency.

The data indicates that there is a pickup of a couple of efficiency points when the motor is run under a minimum stator current condition as opposed to a minimum motor loss condition. These results demonstrate that perhaps the best algorithm to achieve the highest system efficiency is not being employed in current motor drive controllers. The results indicate that an iterative controller that perturbs the stator current while monitoring the torque and speed to keep them constant may in fact be the cheapest way to get high efficiency. It is important to remember that these results apply to an induction motor that is running substantially below rated speed and torque. The torque considered low in this analysis is below 10 ft-lb. Toward that end, the following section looks at the next step that this work needs to take to be fully implemented.

5.2. Future Work

Several actions can be taken in the future to extend and add to this work. First and probably most basic is to increase the cooling capability on the test set so that the drive could be ran at slightly higher torque and speed combination. This would also require a more potent power supply. Next and perhaps more importantly is to alter the control of the inverter to allow the inverter frequency to be controlled in much tighter increments. This would allow the rotor speed to be set constant while the electrical frequency is varied which is more representative of the simulated model. While the current technique works and valuable insight was gathered, the ability to maintain constant output power would greatly enhance the significance of the results and would better identify the magnitude of efficiency savings for the system by running at different slip frequency. Next, the control loop on the motor drive should be closed in order to implement a maximum torque per ampere control strategy, which would help the total system efficiency as shown above. As far as the simulation effort goes, a deeper understanding of the stray load losses is needed in order to port the model to higher speeds and torque levels.

References

[1] S.A. Nasar, “Electric Energy Systems,” Prentice Hall, 1996.

[2] “Integrated Cooling System for Induction Motor Traction Drives”, CARAT Program phase one final report, Charles E. Konrad, November 7, 1999.

[3] M. Ta-Cao, Y. Hori, “Convergence Improvement of Efficiency-Optimized Control of Induction Motor Drives,” IEEE Transactions, May 2000. pp. 1662-1669.

[4] D. Neacsu, K. Rajashekara, “Comparative Analysis of Torque-Controlled IM Drives with Applications in Electric and Hybrid Vehicles,” IEEE Transactions on Power Electronics, Vol. 16 No2, March 2001, pp. 244-247.

[5] O. Wasynczuk, et. al, “A Maximum Torque per Ampere Control Strategy for Induction Motor Drives,” IEEE Transactions on Energy Conversion, Vol. 13, No. 2, June 1998, pp. 163-169.

[6] J. Jung and K. Nam, “A Vector Control Scheme for EV Induction Motors with a Series Loss Model,” IEEE Transactions on Industrial Electronics, Vol. 45, No. 4, August 1998, pp. 617-629.

[7] E. Hall, et. al, “Optimum Speed Ratio of Induction Motor Drives for Electrical Vehicle Propulsion,” IEEE Transactions, February 2001, pp. 371-377.

[8] M.H. Shin, D.S. Hyun, and S.B Cho, “Maximum Torque Control of Stator Flux-Oriented Induction Machine Drive in the Field Weakening Region,” IEEE Transactions, May, 2000, pp. 1461-1467.

[9] J.K. Seok and S.K Sul, “Optimal Flux Selection of an Induction Machine for Maximum Torque Operation in Flux-Weakening Region,” IEEE Transactions on Power Electronics, Vol. 14, No. 4, July 1999, pp. 700-708.

[10] G. Rafajloski, E. Ratz, and D, Manov, “Modeling Analysis and Simulation of Motor Parameter Variation in Vector Controlled Electrical Drives,” IEEE Transactions, May 1997, pp. 1475-1479.

[11] S.H Kim, S.K Sul, and M.H. Park, “Maximum Torque Control of an Induction Machine in the Field Weakening Region,” IEEE Transactions, 1993, pp. 401-407.
[12] F. Briz, et. al., “Current and Flux Regulation in Field-Weakening Region Operation,” IEEE Transactions on Industry Applications, Vol. 37, No. 1 January, 2001, pp. 42-50.
[13] X. Xu and D. Novotny, “Selection of the Flux Reference for Induction Machine Drives in the Field Weakening Region,” IEEE Transactions on Industry Applications, Vol. 28, No. 6, November, 1992, pp. 1353-1358.
[14] G. El-Saady, et. al., “ A High Performance induction Motor Drive System Using Fuzzy Logic Controller,” IEEE Transactions, June, 1994, pp. 1058-1061.
[15] M.R. Udayagiri and T.A. Lipo, “Simulation of Inverter Fed Induction Motors Including Core Losses,” IEEE Transactions, pp. 232-237.
[16] J.C. Moreira, T.A. Lipo, V. Blasko, “Simple Efficiency Maximer for an Adjustable Frequency induction Motor Drive,” IEEE Transactions on Industry Applications, Vol. 27, No. 5, September, 1991, pp. 940-946.
[17] L. Harnefors, “Design and Analysis of General Rotor-Flux-Oriented Vector Control Systems,” IEEE Transactions of Industrial Electronics, Vol. 48, No. 2, April 2001, pp. 383-390.
[18] A.F. Burke, “Electric Vehicle Propulsion and Battery Technology 1975-1995,” IEEE Transactions, pp. 119-135.
[19] K. Matsuse, et. al, “High-Response Flux Control of Direct-Field-Oriented Induction Motor with High Efficiency Taking Core Loss into Account,” IEEE Transactions on Industrial Applications, Vol. 35, No. 1, January/February 1999, pp. 62-69.
[20] M.H. Park and S.K. Sul, “Microprocessor-Based Optimal-Efficiency Drive of an Induction Motor,” IEEE Transactions of Industrial Electronics, Vol. 31, No. 1. February, 1984, pp. 390-394.
[21] J. Jung, et. al, “A New Vector Control Scheme Considering Iron Loss for Electric Vehicle Induction Motors,” IEEE Transactions, January 1997, pp. 439-444.
[22] Sung-Don Wee, et. al, “Stator-Flux-Oriented Control of Induction Motor Considering Iron Loss,” IEEE Transactions on Industrial Electronics, Vol. 48, No. 3, June 2001, pp. 602-608.

[23] G. Arias and K. Venkatesan, “Pspice Modeling of an Induction Motor Drive System,” CPES Proceedings 2001, pp. 388-391.
[24] F. Abrahamsen, et. al, “Efficiency Optimized Control of Medium-Size Induction Motor Drives,” IEEE Transactions, May 2000, pp. 1489-1496.
[25] A.K. Adnanes, et. al, “Efficiency Analysis of Electric Vehicles, with Emphasis on Efficiency Optimized Excitation,” IEEE Transactions, 1993, pp. 455-462.
[26] T.C. Huang and M.A. El-Sharkawi, “Induction Motor Efficiency Maximizer using Multi-Layer Fuzzy Control,” IEEE Transactions, 1996, pp. 109-113.
[27] G. Sousa, D. Simonetti, and E. Norena, “ Efficiency Optimization of a Solar Boat Induction Motor Drive,” IEEE Transactions, May, 2000, pp. 1424-1430.
[26] B.K. Bose, “Power Electronics and AC Drives,” Prentice-Hall, 1986.
[27] P.C. Sen, “Principles of Electric Machines and Power Electronics,” John Wiley and Sons, 1989.
[28] M.A. Herwald, “Control Design and Analysis of an Advanced Induction Motor Electric Vehicle Drive,” M.S. Thesis, Virginia Polytechnic Institute and State University, 1999.
[29] J. Kim, “Analysis of Direct-Soldered Power Module / Heat Sink Thermal Interface for Electric Vehicle Applications,” M.S. Thesis, Virginia Polytechnic Institute and State University, 2001.

Appendix A

n_s=1039RPM T=5 ft-lb

Torque	Loaded Speed	VLL Motor	I Line Motor	Pwr In Motor	Vdc	Idc meas R=0.25mOhm
(inlb)	(RPM)	(rms Volts L-L)	(rms A/Phase)	(Watts)	(V)	(mV)
59.8	928	12.00	55.11	858	18.9	14.93
59.8	946	12.77	51.06	848	19.84	13.71
59.8	967	13.90	46.70	839	21.2	12.34
59.8	976	14.71	44.62	841	22.2	11.56
59.8	981	15.17	43.82	845	22.7	11.23
59.8	985	15.60	42.93	845	23.3	10.86
59.8	989	16.16	42.13	849	23.94	10.45
59.8	993	16.60	41.59	851	24.48	10.21
59.8	996	17.09	41.14	854	25.1	9.96
59.8	998	17.47	40.84	857	25.5	9.72
59.8	1001	17.90	40.67	862	26.06	9.59
59.8	1003	18.37	40.51	866	26.6	9.32
59.8	1004	18.73	40.51	871	27.06	9.22
59.8	1006	19.11	40.54	877	27.49	9.08
59.8	1008	19.65	40.67	884	28.15	8.90
59.8	1010	20.04	40.77	887	28.63	8.78
59.8	1011	20.41	41.01	895	29.08	8.65
59.8	1012	20.80	41.29	900	29.54	8.59
59.8	1013	21.39	41.89	912	30.25	8.43
59.8	1014	21.90	42.50	921	30.90	8.32

n_s=1037RPM T=10 ft-lb

Torque	Loaded Speed	VLL Motor	I Line Motor	Pwr In Motor	Vdc	Idc meas R=0.25mOhm
(inlb)	(RPM)	(rms Volts L-L)	(rms A/Phase)	(Watts)	(V)	(mV)
119.97	907	16.41	78.35	1740	25.4	21.50
119.97	925	17.25	73.68	1710	26.4	20.02
119.97	937	17.97	70.43	1692	27.28	18.99
119.97	946	18.63	67.92	1682	28.1	18.17
119.97	954	19.23	66.01	1678	28.8	17.45
119.97	962	19.94	64.11	1675	29.67	16.77
119.97	970	20.81	62.31	1678	30.7	16.10
119.97	976	21.57	61.12	1683	31.66	15.50
119.97	982	22.46	60.15	1690	32.75	14.90
119.97	986	23.20	59.80	1702	33.67	14.46
119.97	992	24.19	60.03	1725	34.83	13.98
119.97	995	24.96	60.70	1746	35.75	13.80
119.97	998	25.72	61.87	1770	36.65	13.50
119.97	1000	26.32	63.22	1796	37.4	13.45
119.97	1003	27.30	66.42	1854	38.6	13.40
119.97	1005	28.15	70.30	1924	39.64	13.40

n_s=1037RPM T=15 ft-lb

Torque	Loaded Speed	VLL Motor	I Line Motor	Pwr In Motor	Vdc	Idc meas R=0.25mOhm
(inlb)	(RPM)	(rms Volts L-L)	(rms A/Phase)	(Watts)	(V)	(mV)
180.12	913	20.50	90.30	2626	31.27	25.24
180.12	928	21.50	86.46	2610	32.47	23.72
180.12	939	22.38	83.63	2597	33.54	22.60
180.12	948	23.20	81.38	2586	34.52	21.65
180.12	957	24.08	79.46	2581	35.6	20.80
180.12	965	25.11	77.97	2590	36.84	19.97
180.12	970	25.82	77.56	2609	37.7	19.50
180.12	975	26.64	77.66	2641	38.7	19.10
180.12	980	27.46	78.62	2696	39.7	18.70
180.12	983	28.33	80.57	2782	40.73	18.60
180.12	988	29.25	83.79	2922	41.82	18.56
180.12	991	30.09	87.74	3104	42.87	18.71

n_s=2023RPM T=5 ft-lb

Torque	Loaded Speed	VLL Motor	I Line Motor	Pwr In Motor	Vdc	Idc meas R=0.25mOhm
(inlb)	(RPM)	(rms Volts L-L)	(rms A/Phase)	(Watts)	(V)	(mV)
59.8	1850	18.30	66.56	1607	27.7	17.78
59.8	1863	18.78	64.30	1598	28.23	17.12
59.8	1881	19.50	61.12	1581	29.1	16.21
59.8	1897	20.35	58.28	1576	30.18	15.40
59.8	1910	21.25	55.56	1569	31.29	14.62
59.8	1919	21.93	53.76	1565	32.15	14.09
59.8	1927	22.57	52.31	1563	32.96	13.65
59.8	1934	23.30	50.63	1557	33.88	13.11
59.8	1941	23.98	49.46	1559	34.73	12.73
59.8	1946	24.72	48.19	1558	35.66	12.31
59.8	1945	24.86	48.08	1562	35.9	12.29
59.8	1951	25.65	46.69	1555	36.89	11.80
59.8	1955	26.22	45.95	1556	37.6	11.55
59.8	1957	26.63	45.47	1558	38.14	11.37
59.8	1960	27.20	44.95	1563	38.87	11.17
59.8	1962	27.67	44.49	1566	39.47	10.99
59.8	1964	27.99	44.08	1562	39.85	10.83
59.8	1967	28.61	43.5	1562	40.64	10.59
60.15	1969	28.96	43.40	1572	41.09	10.51
60	1970	29.23	43.17	1573	41.42	10.43
59.8	1973	30.04	42.44	1568	42.45	10.10
59.8	1974	30.43	42.33	1576	42.93	10.01
59.8	1976	30.75	42.15	1575	43.33	9.92
59.8	1979	31.64	41.72	1579	44.45	9.65
60.1	1980	32.31	41.61	1592	45.29	9.49
59.8	1983	33.02	41.20	1585	46.17	9.26
59.8	1985	33.97	41.06	1594	47.35	9.05
60.5	1986	34.36	41.23	1610	47.86	9.03
60.5	1988	35.15	41.21	1618	48.83	8.87
59.8	1990	35.86	41.06	1612	49.69	8.67
59.5	1991	36.65	40.97	1611	50.67	8.46
60.5	1994	38.21	41.56	1645	52.63	8.31
60.5	1995	39.30	41.94	1656	54.01	8.11
59.8	1997	40.39	42.26	1657	55.34	7.89
60.5	1998	40.99	42.76	1676	56.10	7.89
60.1	1999	41.85	43.30	1684	57.18	7.78
60.5	2000	42.84	44.04	1696	58.40	7.62
60.1	2001	43.85	44.92	1706	59.65	7.53
60.1	2002	44.48	45.61	1721	60.44	7.48

n_s=2023RPM T=10 ft-lb

Torque	Loaded Speed	VLL Motor	I Line Motor	Pwr In Motor	Vdc	Idc meas R=0.25mOhm
(inlb)	(RPM)	(rms Volts L-L)	(rms A/Phase)	(Watts)	(V)	(mV)
119.97	1861	27.73	84.73	3161	40.89	22.53
119.97	1866	27.94	83.90	3155	41.08	22.31
119.97	1872	28.32	82.60	3148	42.52	21.92
119.97	1881	28.81	81.06	3141	42.16	21.49
119.97	1890	29.44	79.21	3131	42.91	20.89
119.97	1898	30.07	77.42	3123	43.7	20.41
119.97	1907	30.82	75.56	3116	44.63	19.79
119.97	1915	31.77	73.32	3108	45.83	19.10
119.97	1923	32.59	71.60	3101	46.88	18.55
119.97	1928	33.26	70.35	3102	47.7	18.15
119.97	1930	33.91	69.18	3098	48.53	17.75
119.97	1933	34.66	68.05	3104	49.51	17.39
119.97	1935	35.35	67.09	3108	50.43	17.05
119.97	1940	36.11	65.99	3107	51.36	16.67
119.97	1942	36.79	65.23	3113	52.21	16.38
119.97	1946	37.42	64.48	3113	53	16.10
119.97	1948	37.89	64.04	3116	53.67	15.89
119.97	1951	38.56	63.39	3119	54.41	15.63
120.31	1953	39.18	62.98	3125	55.23	15.39
119.97	1956	39.65	62.57	3125	55.83	15.20
120.31	1959	40.33	62.11	3131	56.68	14.95
120.31	1961	41.12	61.71	3138	57.67	14.73
119.97	1963	41.67	61.42	3139	58.35	14.51
119.97	1965	42.28	61.24	3145	59.13	14.29
120.31	1967	42.89	61.18	3156	59.89	14.16
119.97	1969	43.59	60.97	3157	60.75	13.91
120.31	1971	44.22	61.09	3173	61.55	13.77
120.31	1973	44.97	61.15	3181	62.44	13.65
120.1	1975	45.95	61.40	3194	63.69	13.39
119.97	1977	46.81	61.79	3206	64.71	13.19
120.31	1979	47.56	62.32	3223	65.67	13.08
119.97	1981	48.46	63.13	3242	66.79	12.96
120.31	1982	49.25	64.09	3268	67.77	12.79
119.97	1984	50.21	65.35	3287	68.95	12.70
120.31	1986	51.27	67.29	3330	70.29	12.63
119.97	1987	52.24	69.40	3357	71.47	12.47
120.31	1989	53.47	72.76	3421	73.02	12.44

n_s=3061RPM T=5 ft-lb

Torque	Loaded Speed	VLL Motor	I Line Motor	Pwr In Motor	Vdc	Idc meas R=0.25mOhm
(inlb)	(RPM)	(rms Volts L-L)	(rms A/Phase)	(Watts)	(V)	(mV)
60.156	2902	28.07	63.73	2375	40.62	16.56
60.156	2919	29.49	60.43	2365	42.44	15.68
60.156	2932	30.58	58.20	2359	43.80	15.02
60.156	2939	31.40	56.82	2362	44.88	14.62
60.156	2951	32.69	54.61	2354	46.53	13.97
60.156	2959	33.79	53.00	2352	47.91	13.48
60.156	2969	35.38	50.94	2349	49.95	12.83
60.156	2978	36.76	49.45	2353	51.72	12.35
60.156	2981	37.33	48.84	2351	52.43	12.14
60.156	2985	38.30	47.98	2356	53.70	11.83
60.156	2989	39.25	47.13	2355	54.91	11.53
60.156	2993	40.20	46.33	2354	56.12	11.24
60.156	2998	41.39	45.56	2360	57.66	10.95
60.156	3001	42.35	44.92	2360	58.88	10.67
60.156	3003	42.86	44.69	2366	59.55	10.58
60.156	3006	43.68	44.29	2370	60.59	10.39
60.156	3008	44.60	43.78	2368	61.77	10.15
60.156	3010	45.48	43.52	2376	62.88	10.00
60.156	3013	46.42	43.11	2377	64.08	9.79
59.81	3017	48.03	42.61	2381	66.12	9.48
59.81	3018	48.77	42.44	2386	67.06	9.35
60.156	3019	49.63	42.38	2398	68.13	9.23
60.156	3021	50.45	42.25	2403	69.18	9.10
60.156	3022	51.13	42.15	2407	70.04	8.99
60.156	3024	52.22	42.06	2414	71.42	8.81
60.156	3025	52.99	42.01	2419	72.39	8.71
60.156	3027	53.51	41.95	2416	73.08	8.64
60.156	3028	54.38	41.99	2425	74.17	8.53
60.156	3029	55.26	42.02	2431	75.30	8.39
60.156	3030	56.03	42.15	2443	76.28	8.31
60.156	3031	57.01	42.25	2450	77.53	8.19
60.156	3032	57.74	42.34	2453	78.44	8.09
59.81	3033	58.71	42.52	2455	79.70	7.99
60.156	3034	59.63	42.79	2466	80.89	7.89
59.81	3035	60.11	42.86	2462	81.45	7.81
60.156	3036	61.21	43.36	2488	82.90	7.75
59.81	3037	62.06	43.60	2485	83.97	7.62

n_s=3061RPM T=10 ft-lb

Torque	Loaded Speed	VLL Motor	I Line Motor	Pwr In Motor	Vdc	Idc meas R=0.25mOhm
(inlb)	(RPM)	(rms Volts L-L)	(rms A/Phase)	(Watts)	(V)	(mV)
119.97	2897	39.92	87.12	4670	57.1	22.73
119.97	2907	41.02	84.78	4664	58.54	22.02
119.97	2915	42.06	82.62	4653	59.84	21.43
119.97	2922	43.04	80.68	4659	61.08	20.88
119.97	2931	44.28	78.65	4644	62.67	20.26
119.97	2936	45.01	77.40	4639	63.62	19.90
119.97	2941	45.93	76.03	4639	64.76	19.47
119.97	2948	47.06	74.40	4636	66.26	18.97
119.97	2951	47.75	73.48	4636	67.15	18.68
120.1	2955	48.54	72.48	4635	68.15	18.36
119.97	2960	49.46	71.29	4627	69.32	17.97
119.97	2965	50.56	70.13	4630	70.73	17.55
120.31	2970	51.70	69.03	4639	72.22	17.20
120.31	2974	52.73	68.12	4641	73.52	16.86
119.97	2976	53.24	67.54	4633	74.18	16.67
119.97	2979	54.01	66.90	4636	75.18	16.43
119.97	2981	54.81	66.28	4638	76.23	16.17
119.97	2984	55.47	65.81	4642	77.07	16.00
120.31	2987	56.68	65.09	4654	78.65	15.71
120.31	2990	57.40	64.64	4655	79.58	15.47
119.97	2991	58.00	64.21	4650	80.37	15.30
120.1	2994	58.81	63.87	4659	81.42	15.12
120.31	2996	59.79	63.45	4666	82.67	14.88
120.31	2998	60.72	63.18	4680	83.89	14.69
120.31	3001	61.93	62.82	4690	85.43	14.45
120.31	3003	62.75	62.59	4691	86.48	14.23
120.31	3005	63.73	62.50	4713	87.69	14.10
119.97	3007	64.49	62.23	4701	88.65	13.91
119.97	3008	65.35	62.19	4707	89.70	13.72
120.1	3010	66.42	62.25	4726	91.10	13.55
120.31	3012	67.56	62.44	4746	92.50	13.37
119.97	3013	68.25	62.47	4742	93.34	13.22
120.31	3015	69.18	62.86	4772	94.54	13.15
119.97	3016	70.10	63.06	4771	95.68	12.96
119.97	3017	70.97	63.45	4785	96.79	12.81
120.31	3018	71.44	63.72	4797	97.38	12.80
120.31	3019	72.37	64.30	4811	98.55	12.68

n_s=4043RPM T=5 ft-lb

Torque	Loaded Speed	VLL Motor	I Line Motor	Pwr In Motor	Vdc	Idc meas R=0.25mOhm
(inlb)	(RPM)	(rms Volts L-L)	(rms A/Phase)	(Watts)	(V)	(mV)
59.8	3831	31.48	75.17	3119	45.5	19.40
59.8	3852	32.68	72.06	3113	47.02	18.60
59.8	3865	33.47	69.91	3097	48.01	18.03
59.8	3884	34.82	66.87	3084	49.7	17.22
59.8	3896	35.76	64.91	3076	50.95	16.68
59.8	3900	36.72	63.30	3080	52.17	16.27
59.8	3910	37.75	61.63	3080	53.45	15.80
59.8	3919	38.91	59.83	3076	54.96	15.29
59.8	3926	39.90	58.38	3074	56.25	14.87
59.8	3934	40.93	56.99	3071	57.56	14.47
59.8	3943	42.41	55.20	3071	59.47	13.93
59.8	3949	43.50	53.93	3065	60.87	13.55
59.8	3953	44.46	52.91	3064	62.1	13.24
59.8	3959	45.62	51.83	3066	63.6	12.90
59.8	3963	46.55	50.99	3066	64.81	12.64
59.8	3968	47.90	49.88	3068	66.55	12.26
59.8	3971	48.94	49.16	3073	67.89	12.01
59.8	3976	50.03	48.42	3076	69.32	11.76
59.8	3979	51.17	47.64	3075	70.78	11.50
59.8	3983	52.41	46.91	3077	72.40	11.20
59.8	3986	53.52	46.38	3086	73.85	10.99
59.8	3989	54.63	45.83	3088	75.30	10.78
59.8	3991	55.79	45.26	3088	76.81	10.55
60.156	3994	57.20	44.83	3104	78.64	10.33
60.156	3997	58.22	44.48	3109	79.96	10.16
60.156	3999	59.44	44.06	3108	81.52	9.99
60.156	4002	60.85	43.72	3119	83.36	9.76
60.156	4003	61.70	43.63	3133	84.45	9.67
60.156	4005	63.31	43.30	3142	86.50	9.46
60.156	4007	64.57	42.95	3141	88.10	9.24
59.8	4009	65.92	42.69	3134	89.80	8.99
60.156	4010	67.07	42.66	3153	91.30	8.97
60.156	4012	67.79	42.63	3163	92.22	8.89
60.156	4013	68.83	42.55	3167	93.53	8.73
59.8	4014	69.85	42.45	3166	94.82	8.57
59.8	4015	71.28	42.34	3164	96.63	8.41
60.156	4016	72.39	42.54	3194	98.05	8.39
59.8	4018	73.95	42.52	3190	100.02	8.19
59.8	4019	74.87	42.59	3195	101.22	8.12
60.156	4020	76.44	42.87	3218	103.20	7.99
59.8	4021	77.21	42.88	3205	104.15	7.88
59.8	4022	78.35	43.10	3217	105.60	7.78

Appendix B

Losses as a function of slip for a fixed speed and torque, varying the stator voltage and slip frequency to obtain the desired speed and torque.

Rated Voltage is 1.425 volts (line-line)/Hz
At 60 Hz, rated volts (line-line) is 85.5 volts & 50 volts (line-neutral)

$R1 := 0.012 \qquad X1 := 0.0149i$
$R2 := 0.0125 \qquad X2 := 0.0157i$

MOTOR MAGNETIZING BRANCH IMPEDANCES :

First find Magnetizing branch resistance as a function of voltage:

$i := 0 .. 17$
$A := READPRN("MOTORMAG.TXT")$ Uses the no-load test data at 60 Hz.

$i := 0 .. 17$
$v(i) := 5 \cdot (i + 1) \qquad RM(i) := A_{(i,0)} \qquad XM(i) := A_{i,1}$

$V_i := 5 \cdot (i + 1)$

$RM_i := A_{i,0}$

$RS := cspline(V, RM)$

$RM(v) := interp(RS, V, RM, v)$

Core Resistance as a function of voltage is RM(v): $RM(60) = 14.5$

Find the 60 Hz. Magnetizing reactance as a function of the voltage across the magnetizing branch

$XM_i := A_{i,1}$

$XMS := cspline(V, XM)$

$XM(v) := interp(XMS, V, XM, v)$

Core Reactance as a function of voltage is XM(v): $v := 5, 6 .. 90$

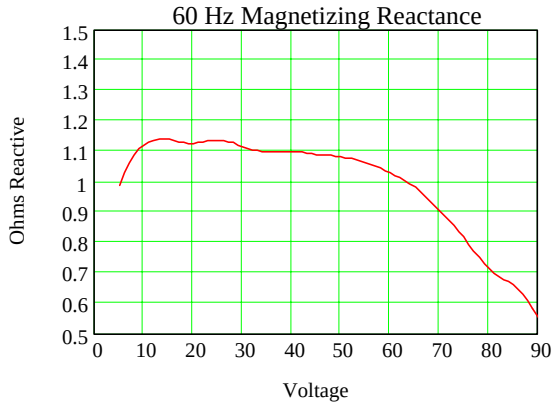

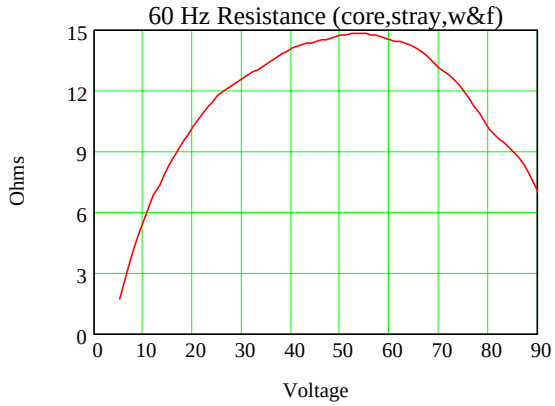

Maximum Stator Volts (Vmax)(was 100): $Vmax := 150$ Line-Neutral @ 60 H:

Removed Windage & Friction from stray loss: $StrayLoss(j) := 15$ Watts

$j := 0.15, 0.20 .. 5$ Note that "j" will be used as the slip frequency

$Speed := 3000$

$Torque := 5$

Find the per unit slip (s):

$SlipFrequency(j) := j$

$$LineFrequency(j) := \frac{Speed}{3600} \cdot 60 + SlipFrequency(j)$$

$$s(j) := \frac{SlipFrequency(j)}{LineFrequency(j)}$$

Find the maximum stator voltage to avoid saturation:

$$Vmax(j) := \frac{LineFrequency(j)}{60} \cdot Vmax$$

Find the Output Power for one (Power in Watts):

$$Power(j) := \frac{(746 \cdot Torque \cdot Speed)}{5252}$$ Watts

Next find the rotor current (I2):

$$I2(j) := \left[\frac{s(j) \cdot Power(j)}{3 \cdot R2 \cdot (1 - s(j))}\right]^{0.5}$$ amps

Next find the total rotor impedance per phase (ZR in ohms)

$$RotorImpedance(j) := \frac{R2}{s(j)} + \frac{LineFrequency(j)}{60} \cdot X2$$

$$ZR(j) := RotorImpedance(j)$$

Find the voltage across the magnetizing branch (VM in volts):

$$VM(j) := I2(j) \cdot ZR(j)$$

$$MagVolts(j) := |VM(j)|$$

If the Mag Volts is greater than Vmax, then set equal to Vmax to avoid at saturation:

$$VM(j) := if(MagVolts(j) < Vmax(j), MagVolts(j), Vmax(j))$$

Now correct angle of rotor current for Mag Volts being zero reference:

$$I2(j) := \frac{VM(j)}{ZR(j)}$$

$$RotorCurrent(j) := |I2(j)|$$

Find magnetizing current (IM in amps): Magnetude of rotor current (I2 in amps RMS

$$volts(j) := |VM(j)|$$

Magnetude Need to adjust RM for frequency.

$$RMA(v) := RM(v) \cdot \left[\frac{60}{LineFrequency\left[\frac{(v - 4)}{10}\right]}\right]^{1.5}$$

$$IM(j) := \frac{VM(j)}{RMA(volts(j))} - \frac{VM(j)}{XM(volts(j)) \cdot \left(\frac{LineFrequency(j)}{60}\right)} \cdot i$$

$$MagCurrent(j) := |IM(j)|$$ Magnetude of magnetizing current (IM in amps RMS

Find Line Current (IS in amps):

$$IS(j) := I2(j) + IM(j)$$

$$StatorCurrent(j) := |IS(j)|$$ Magnetude of stator current (IS in amps RMS):

Find Stator Impedance (ZS in ohms):

$$ZS(j) := R1 + X1 \cdot \frac{LineFrequency(j)}{60}$$

Find Stator Voltage (VS volts line-neutral):

$$VSN(j) := (ZS(j) \cdot IS(j) + VM(j))$$

Find Stator Voltage Magnetude (VS volts line-line)

$$VS(j) := \sqrt{3} \cdot |VSN(j)| \qquad StatorVolts(j) := VS(j)$$

Find Input Power from V*I*cos q $\qquad windage(j) := 200$ watts

$$InputPower(j) := 3 \cdot |VSN(j)| \cdot |IS(j)| \cdot \cos(\arg(VSN(j)) - \arg(IS(j))) + StrayLoss(j) + windage(j) \cdot \left(\frac{LineFrequency(j)}{50}\right)$$

Next find the efficiency:

$$Efficiency(j) := \frac{Power(j)}{InputPower(j)}$$

Find the Power Factor:

$$VoltAmps(j) := |VSN(j)| \cdot |IS(j)| \cdot 3$$

$$PowerFactor(j) := \frac{InputPower(j)}{VoltAmps(j)}$$

$$CoreLoss(j) := \frac{(|VM(j)|)^2 \cdot 3}{RM(volts(j))}$$

$$StatorVolts(j) := |VS(j)|$$

$$StatorCU(j) := (|IS(j)|)^2 \cdot R1 \cdot 3$$

$$RotorCU(j) := (|I2(j)|)^2 \cdot R2 \cdot 3$$

$$InputPower(j) := Power(j) + CoreLoss(j) + StatorCU(j) + RotorCU(j) + StrayLoss(j) + windage(j) \cdot \left(\frac{LineFrequency(j)}{50}\right)$$

$$Eff(j) := 100 \cdot Efficiency(j)$$

$$TotalLoss(j) := CoreLoss(j) + StatorCU(j) + RotorCU(j) + StrayLoss(j) + windage(j) \cdot \left(\frac{LineFrequency(j)}{50}\right)$$

Vita

Heath Kouns graduated salutatorian from Bath County High School in 1995 in Virginia. He then attended Virginia Tech and completed a B. S. degree in Electrical Engineering in 2000. He was accepted into the 5 year BS/MS program and this thesis competes work towards his M.S. degree. Heath's research interests included inverter control for induction motor drives and product development. Heath also worked part time doing product development consulting for a variety of companies. Heath began work as a Product Engineer and Project Manager for Northrop Grumman Poly-Scientific in Blacksburg, VA in late summer of 2001. His work there deals with fiber optic component development for the telecommunications industry.